

## Accepted Manuscript

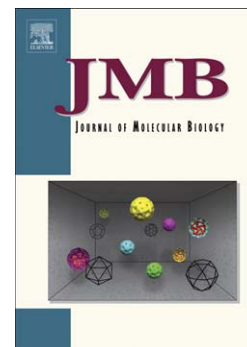
High-resolution mapping of the folding transition state of a WW domain

Kapil Dave, Marcus Jäger, Houbi Nguyen, Jeffery W. Kelly, Martin Gruebele

PII: S0022-2836(16)00113-3  
DOI: doi: [10.1016/j.jmb.2016.02.008](https://doi.org/10.1016/j.jmb.2016.02.008)  
Reference: YJMBI 64994

To appear in: *Journal of Molecular Biology*

Received date: 8 October 2015  
Revised date: 1 February 2016  
Accepted date: 7 February 2016



Please cite this article as: Dave, K., Jäger, M., Nguyen, H., Kelly, J.W. & Gruebele, M., High-resolution mapping of the folding transition state of a WW domain, *Journal of Molecular Biology* (2016), doi: [10.1016/j.jmb.2016.02.008](https://doi.org/10.1016/j.jmb.2016.02.008)

This is a PDF file of an unedited manuscript that has been accepted for publication. As a service to our customers we are providing this early version of the manuscript. The manuscript will undergo copyediting, typesetting, and review of the resulting proof before it is published in its final form. Please note that during the production process errors may be discovered which could affect the content, and all legal disclaimers that apply to the journal pertain.

Submitted to: J. Mol. Biol.

## High-resolution mapping of the folding transition state of a WW domain

Kapil Dave<sup>†,‡</sup>, Marcus Jäger<sup>§,‡</sup>, Houbi Nguyen<sup>†</sup>, Jeffery W. Kelly<sup>§</sup> and Martin Gruebele<sup>†,¶,\*</sup>

<sup>†</sup>Center for Biophysics and Computational Biology, University of Illinois at Urbana-Champaign, Urbana, IL 61801 USA. <sup>§</sup>Department of Chemistry and The Skaggs Institute for Chemical Biology, The Scripps Research Institute, 10550 North Torrey Pines Road BCC255, La Jolla, CA 92037, USA. <sup>¶</sup>Department of Physics and Department of Chemistry, University of Illinois at Urbana-Champaign, Urbana, IL 61801 USA

\*Corresponding author

<sup>‡</sup> These authors contributed equally to the work

ABSTRACT: Fast-folding WW domains are among the best-characterized systems for comparing experiments and simulations of protein folding. Recent microsecond-resolution experiments and long (totaling milliseconds) single-trajectory modeling have shown that even mechanistic changes due to mutation in folding kinetics can now be analyzed. Thus, a comprehensive set of experimental data would be helpful to benchmark the predictions made by simulations. Here, we use T-jump relaxation in conjunction with protein engineering and report  $\Phi$  values as indicators for folding transition state structure for 65 side chain, 7 backbone hydrogen bond and 6 loop 1 deletion and/or insertion mutants of the 34-residue hPin1 WW domain. 45 cross-validated consensus mutants could be identified that provide structural constraints for transition state structure within all substructures of the WW domain fold (hydrophobic core, loop 1, loop 2,  $\beta$  sheet). We probe the robustness of the two hydrophobic clusters in the folding transition state, discuss how local backbone disorder in the native state can lead to non-classical  $\Phi_M$  values ( $\Phi_M > 1$ ) in the rate-determining loop 1 substructure, and conclusively identify mutations and positions along the sequence that perturb the folding mechanism from loop 1-limited towards loop 2-limited folding.

---

\*Correspondence:

M. Gruebele, Tel.: 217-333-1624; E-mail: mgruebel@illinois.edu

## Introduction

WW domains are  $\beta$  sheet modular protein domains of 30-65 residues in length that modulate specific interactions with proline-rich protein ligands. WW domains have proven to be an excellent model for ultrafast folding experiments, for mechanistic experimental studies on the folding of a simple  $\beta$  sheet structure, and for benchmarking computational folding scenarios [1-3].

The best characterized natural WW domains to date are the hPin1 WW domain from human peptidyl-prolyl *cis-trans* isomerase Pin1 [3], and the FBP28 WW domain from formin-binding protein 28 [4], with limited data available for a third WW domain, the hYAP65 WW domain from human Yes-Kinase associated kinase [5]. Mutational  $\Phi_M$  value analysis suggest that formation of loop 1 in WW domains is mostly rate limiting ( $\Phi_M$  values  $> 0.80$ ) [6].

In FBP28 WW and hYap65 WW, the N-terminal loop 1 sequence folds into a 5-residue type-I G-bulge turn, the statistically preferred conformation among WW domains. The longer, intrinsically disordered 6-residue loop 1 in hPin1 WW appears to have been selected for function. Its unusual loop conformation (type II-turn intercalated in a 6-residue loop) may position the side chains of residues S16 and R17 for optimal ligand binding [7]. Replacing the hPin1 loop 1 with the turn of FBP28 WW to make the FiP WW domain increases stability by up to 7 kJ/mole and speeds up folding from  $\sim 80 \mu\text{s}$  to  $\sim 13 \mu\text{s}$ , but compromises function [7]. A similar frustration of folding by function has also been observed in other cases, such as frataxin [8].

For WW domains with their loop 1 substructure optimized for folding thermodynamics and kinetics, formation of loop 2 becomes competitive as the rate-limiting step for folding. Indeed, further optimization of the loop 2 sequence in FiP (FiP N30G/A31T/Q33T, FiP-GTT hereafter) produced a WW domain with a folding relaxation time of  $\sim 4 \mu\text{s}$ , approaching the speed limit for folding [9].

Here we report an in-depth study of temperature jump kinetics for 78 mutants of the hPin1 WW domain (Table 1) that also includes data from two more limited, previous  $\Phi$  value analyses [6, 7, 10, 11]. 45 mutants were amenable for  $\Phi_M$  value analysis, providing energetic constraints for structural mapping of the folding transition state of hPin1 WW. Multiple side chain substitutions at some key sequence positions (e.g. within the hydrophobic cores or loop 2) allow us to calculate error-weighted average  $\Phi_M$  values that are more likely to be a robust representation of transition state vs. native state free energy changes than single (e.g. Ala) substitutions. We also identify substitutions that are not suitable for  $\Phi_M$  value analysis, and discuss the reasons. This approach has been used by Davidson and co-workers to investigate ‘conservatism’ of substitutions at several sites of the SH3 domain [12].

Although wild type hPin1 WW and its variants fold more slowly than the redesigned loop 1 variant FiP, their folding rates are still in the microsecond range that is now within the reach of fast folding simulations. As computation of folding in the 50-500  $\mu$ s range becomes feasible, we believe that the data presented in this study will prove to be a rich resource for detailed comparisons, providing constraints on mechanisms and rate changes deduced from molecular dynamics simulations, which are still debated in the literature [9, 13-15].

## RESULTS AND DISCUSSION

After a brief review of hPin1 WW structure and native state interactions (Fig. 1, section 1), we begin our discussion of the results in section 2 with the mutational phi-value ( $\Phi_M$ ) analysis, focusing on which mutants are likely to be reliable reporters for transition state structure (Fig. 2). Next, a temperature-dependent phi-value ( $\Phi_T$ ) analysis is used in section 3 to identify mutations that perturb the folding mechanism and whose perturbing effect escapes detection by inspection of the mutational  $\Phi_M$  values only (Fig. 3). The consensus set of 39 non-perturbing mutants with reliable  $\Phi_M$  values is employed in section 4 to analyze the transition state structure of hPin1 WW (Figs 4-7). Section 5 looks at various loop 1 insertion and deletion variants within the rate-limiting loop 1 substructure (Fig. 8). A hypothetical “hybrid”  $\Phi_M$  map

for the ultrafast folding hPin1 WW variant FiP (Fig. 9) to benchmark recent molecular dynamics simulations concludes the paper.

## 1. Overview of hPin1 WW structure and native state interactions

Two types of interactions help stabilize and specify the three-stranded  $\beta$  sheet structure of the hPin1 WW domain. The first type is mediated by the side chains of conserved hydrophobic residues that form two segregated hydrophobic clusters, one on each side of the  $\beta$  sheet (Fig. 1a). The second type of interaction involves a network of 10 backbone-backbone and 4 backbone-side chain hydrogen bonds (Fig. 1b).

Hydrophobic cluster 1 is formed by the side chains of residues L7, P8, W11, Y24 and P37. The N-terminal Trp (W11 in hPin1 WW) and the C-terminal Pro (P37 in hPin1 WW) are absolutely conserved in WW domains. Mutation of residues W11, Y24 and P37 to Ala or Leu in hPin1 WW results in partially unfolded, or fully unfolded protein, even at low temperature (4° C) (Fig. 1c and [10]). As hydrophobic cluster 1 does not contribute to ligand binding, these medium-long range side chain interactions appear to have evolved to maximize thermodynamic stability of hPin1 WW, rather than its biological function.

Hydrophobic core 2 lies on the ligand-binding face of the three-stranded  $\beta$  sheet, and is formed by the side chains of residues R14, Y23 and F25 (Fig. 1a). These residues are only moderately conserved in WW domains, presumably because hydrophobic core 2 contributes to ligand binding. Ala mutations of residues 14, 23 and 25 in hPin1 WW, although severely destabilizing the native state ( $\Delta\Delta G_f \sim 9$  kJ/mole) (Fig. 1c), allow folding into the native state structure under the most favorable folding conditions (4 °C).

Using amide-to-ester mutagenesis, we showed that the degree of destabilization of the native state upon eliminating a backbone hydrogen bond is strongly context-dependent [16]. Hydrogen bonds near the two loop substructures are less influential than hydrogen bonds that are protected within a hydrophobic core. The side chain amino group of N26 ( $\beta$  strand 2) forms

a hydrogen bond with the backbone carbonyl group of P9 and to the indole ring of W11, thus linking  $\beta$  strands 1 and 2 of the three-stranded  $\beta$  sheet. Like the hydrophobic core 1 residues (W11, Y24 and P37 in hPin1 WW), the Asn in strand 2 (N26 in hPin1 WW) is highly conserved among WW domains and N26A or N26L mutations unfold hPin1 WW (Fig. 1c) [10].

## 2. $\Phi_M$ -value analysis

The mutational  $\Phi_M$  value =  $\Delta\Delta G_f^\ddagger / \Delta\Delta G_f$  quantifies changes in the free energy of activation ( $\Delta\Delta G_f^\ddagger$ ) relative to the ground state free energy of folding ( $\Delta\Delta G_f$ ) between wild type and mutant proteins [17, 18] Computational modeling of  $\Phi_M$  values is now possible for WW domains [14, 19], making direct comparisons with experiments achievable.

To obtain accurate  $\Phi_M$  values that truly represent transition state energetics, one must design non-disruptive mutants that differ sufficiently in thermodynamic stability from the wild type reference protein [20-23], but are not so different that the folding landscape is substantially altered. A generally accepted strategy for  $\Phi_M$  value analysis is to use conservative hydrophobic deletion mutations (e.g. Ile/Leu  $\rightarrow$  Val  $\rightarrow$  Ala ; Thr  $\rightarrow$  Ser; Phe  $\rightarrow$  Leu  $\rightarrow$  Ala). This strategy avoids mutants that increase side chain size or introduce new functional groups (i.e. Ser  $\rightarrow$  Thr, Phe  $\rightarrow$  Trp), as well as mutation of solvent-exposed charged residues with long-range electrostatic interactions and/or protein-solvent interactions (e.g. Glu  $\rightarrow$  Ala, Tyr  $\rightarrow$  Phe). Several of the mutations that we employed in our previous side chain  $\Phi_M$  analysis of hPin1 WW [6] do not meet these requirements. This has been discussed in detail in the literature [22].

One in four mutants studied here has a thermodynamic stability very close to wild type hPin1 WW ( $\Delta\Delta G_f < 1$  kJ/mole,  $\Delta T_m < 2.5$  °C, with a typical error in  $T_m$  of 0.5 – 1 °C). These mutants were excluded from the  $\Phi_M$  analysis discussed herein. Their thermodynamic and kinetic data (Table 1) should nonetheless provide a valuable resource for benchmarking upcoming molecular dynamics simulations because most of these mutants fold on the microsecond to millisecond time scale, accessible to all atom explicit [24], implicit [14] and coarse grained simulations [25]. We calculated  $\Phi_M$  values at three representative temperatures (50 °C, 55 °C

and 60 °C) (Table 1), where experimental data was available for almost all mutants without the need for error-prone extrapolation. For some of the more stable loop 1 deletion variants, we only report  $\Phi_M$  values at 55 and/or 60 °C.

### Outliers in the analysis

At 55 °C, the  $\Phi_M$  values of the mutants that potentially qualify for  $\Phi_M$  analysis ( $\Delta\Delta G_f < 1$  kJ/mole and  $\Delta T_m < 2.5$  °C) range from -0.20 (L7I) to 2.56 (S16A) (Fig. 2A, Fig. 2B, Table 1). With the exception of some loop 1 mutants that only slightly destabilize the domain, there is no correlation between the magnitude of a  $\Phi_M$  value and the extent of destabilization ( $\Delta\Delta G_f$  in Fig. 2A and Fig. 2B). Except for mutants E12Q, I28A, and Y23F, the estimated error in  $\Phi_m$  was less than 10 %. A surprisingly high fraction of mutants yield  $\Phi_M$  values that lie outside the classical range of  $\Phi_M$  values (in particular  $\Phi_M > 1$ ). Almost all mutants with non-classical  $\Phi_M$  values map to the hydrophobic core 1 and loop 1 substructures in native hPin1 WW, pointing to the importance of these substructures for transition state energetics. Mutant L7I yields the only negative  $\Phi_M$  value, which is, however, not supported by the L7A and L7V mutations (Fig. 2A). Also the large  $\Phi_M$  value of V22A ( $\beta$  strand 2) can neither be cross-validated by  $\Phi_M$  values of immediate sequence neighbors (R21A/H, Y23L/A) nor by its cross-strand neighbor (M15A,  $\beta$  strand 1). Finally, the  $\Phi_M$  value of Y23F is almost twice as high as the  $\Phi_M$  values of Y23L and Y23A that target the same residue (Fig. 2A). Y23F deletes a solvent-exposed hydroxyl-group that should not affect the side chain packing of hydrophobic core 1. Its unusual  $\Phi_M$  value most likely reports on changes in solvation, rather than packing of the core. Mutants L7I, V22A and Y23F were thus excluded from further analysis.

### Probing key residues for stability by multiple mutations

Several residues critical for thermodynamic stability, i.e. R14, Y23 and F25 that constitute hydrophobic core 2 (Fig. 1a), and T29 in loop 2 of hPin1 WW (Fig. 1b), were probed by multiple mutations (vertical  $\Phi_M$  analysis). We find excellent agreement between the  $\Phi_M$  value of the non-conservative mutants R14F/L and the classical R14A mutant, and the  $\Phi_M$  values of the Leu and Ala mutants of F25 differ by 0.10 units (Fig. 2a, Table 1). This is clear evidence that

hydrophobic cluster 2, although moderately conserved among WW domains, is rather robust towards perturbation by single side chain modifications.

Loop 2 of hPin1 WW is formed by residues H27-N30, and adopts a  $\alpha_R\text{-}\alpha_R\text{-}\alpha_R\text{-}\alpha_L$ , or  $\pi_{\alpha L}$ -conformation, with the first three residues being in a right-handed helical conformation, and N30 being in a left-handed helical conformation. The  $\pi_{\alpha L}$ -conformation is very common among four residue loops and is also found in the homologous hYap65 and FBP28 WW domains. We probed the contribution of T29 to transition state structure and energetics by the three classical mutations T29S/A/G. The non-conservative T29D mutation was also included in the analysis, as T29D is found in the homologous hYap65 WW domain, and T29D was utilized in our first  $\Phi_M$  analysis study of hPin1 WW [6].

The  $\Phi_M$  value of T29A ( $0.49 \pm 0.01$ ) is closest to the error-weighted average  $\Phi_M$  value (0.53), with T29D yielding a slightly lower value ( $\Phi_M = 0.44 \pm 0.01$ ) while T29S ( $\Phi_M = 0.69 \pm 0.02$ ) and T29G ( $\Phi_M = 0.79 \pm 0.01$ ) yielded higher values. Of all these, only the glycine mutant lies more than a standard deviation from the average. We also studied a double-mutant, I28N/T29G, which replaces the base of the helical  $\pi_{\alpha L}$ -turn with a sequence (Asn-Gly) that has a high propensity to form a tight 4-residue type-I' turn, a common loop type seen in hairpin structures. I28N/T29G is one of the most destabilized loop 2 mutants ( $\Delta\Delta G_f = 8$  kJ/mol) and has a large  $\Phi_M$  value ( $0.96 \pm 0.01$ ). The larger  $\Phi_M$  value shows that loop 2 can become rate limiting when destabilized, moving the transition state towards the native state. As shown in the next section ( $\Phi_T$  analysis), mutants T29G and I28N/T29G are perturbing mutants in that they shift the folding transition state with respect to wild type hPin1 WW, so both mutants are not reliable reporters of the unperturbed wild type transition state structure.

### **Perturbation of hydrophobic cluster 1 disrupts the folding transition state**

Molecular dynamics simulations of the fast-folding FiP variant of hPin1 WW suggest that hydrophobic cluster 1 is only weakly formed in the transition state. The simulated  $\Phi_M$  values for hydrophobic core 1 residues (L7:  $-0.30 \pm 0.50$ , P8:  $-0.3 \pm 0.1$ , W11:  $\sim 0.4$ , Y24:  $0.32 \pm 0.1$ , P37:  $\sim$

0) suggest that the native W11-Y24 side chain interaction is partially developed in the folding transition state, while other hydrophobic core contacts (e.g. P37 sandwiched between W11 and Y24 (SI Fig. 1)) must develop after crossing the folding barrier [17, 26, 27].

Because of its importance for stability (Fig. 1c), hydrophobic cluster 1 proves to be difficult to map experimentally by  $\Phi_M$  analysis. Even though the negative  $\Phi_M$  value of L7I (within error) agrees with the value from simulations, its  $\Phi_M$  value is not supported by L7A and L7V mutations. Mutating residues W11, Y24 and P37 to either Ala or Leu resulted in unfolded proteins. Mutants P8A, W11F and Y24W, although (severely) destabilized, unfold cooperatively upon heating but yield non-classical  $\Phi_M$  values significantly higher than the  $\Phi_M$  values of other hydrophobic core 1 mutations (L7I/A/V, G10A, Y24F). As the W11F mutant of hPin1 WW folds into a native-like structure with a rigid core (SI Fig. 2), and because the conservative W11F mutation is unlikely to perturb unfolded state structure significantly, the high  $\Phi_M$  value of W11F most likely results from a perturbation of transition state energetics, rather than ground state effects. The Y24W mutation replaces the phenol-moiety of Y24 with the indole ring of Trp. The larger side chain enables “gain-of-interactions” in the denatured and transition state ensembles, as well as steric clashes in the native state that are not present in the wild type protein. The  $\Phi_M$  values of mutants G10A ( $0.57 \pm 0.02$ ) and Y24F ( $0.68 \pm 0.02$ ) agree reasonably well with simulation, but we observed that neither mutation is ideal for transition state mapping. Surface-exposed G10 acts as a hinge residue in hydrophobic core 1 formation, so it does not contribute to the side chain packing of the hydrophobic core *per se*, and Y24F removes a solvent-exposed OH-group without perturbing the side chain packing of the core (SI Fig. 1). Like Y23F in hydrophobic core 2, its  $\Phi_M$  value may primarily report on changes in protein solvation energetics, rather than genuine hydrophobic core contacts. Unlike the disruptive mutations P8A, W11F and Y24W, mutants G10A and Y24F were included in further analysis.

In summary, the large number of disruptive hydrophobic core 1 mutants, the strong effect of the W11F mutation on the hPin1 WW folding kinetics, and the intermediate  $\Phi_M$  values of the

non-disruptive mutants L7A/V/I, G10A and Y24F, suggest that while hydrophobic cluster 1 is only partially structured in the transition state, it is very important for protein stability.

### Non-classical $\Phi_M$ values in loop 1

The intrinsically dynamic loop 1 substructure of hPin1 WW (SI Fig. 3) was probed by both side chain and backbone hydrogen bond mutagenesis. Mutation S16s deletes the backbone hydrogen bond between residues S16 and R21, while mutation R17r weakens, but does not eliminate, the backbone hydrogen bond between residue S16 and S19 (Fig. 1b). Mutants S16G, S19G, S18G/S19G and G20A perturb the native state by changing the backbone entropy.

Supporting our previous hypothesis that loop 1 formation is rate-limiting for hPin1 WW folding, all ten loop 1 mutants exhibit high  $\Phi_M$  values close to or larger than 1 (Fig. 2B). The highest  $\Phi_M$  values were calculated for mutants S16A ( $2.56 \pm 0.02$ ) and S16T ( $1.78 \pm 0.02$ ). The  $\Phi_M$  value of S16A is about twice as high as that of all other loop 1 mutants, and is a clear outlier. From the structure of the folded hPin1 WW domain it is not immediately obvious why S16A would perturb transition state energetics and slow down folding so much, but similar observations have been made with the *fyn*SH3 domain [28], where a T47A substitution produces a  $\Phi_M$  value twice as high as that of T47S and T47G.

Mutants S16G, R17r, S19G, S18G/S19G and G20A all share  $\Phi_M$  values  $> 1$  ( $\Phi_M = 1.14$ - $1.43$ ). Mutants S16G, R17r and G20A are significantly less stable than S19G and S18G/S19G, so at least their non-classical  $\Phi_M$  values cannot be attributed to artifacts due to small differences in the stability between wild type and mutant proteins ( $\Delta\Delta G_f$ ).  $\Phi_M$  values close to 1 are obtained for side chain mutants R21A/H (loop 1/ $\beta$  strand 2 interface) and for mutant S16s that eliminates the backbone hydrogen bond between residues S16 and R21 that closes the 6-residue loop conformation. Except for S16A and S16T, all these mutants are used for further analysis.

### 3. $\Phi_T$ -value analysis

In folding studies that employ chemical denaturants (urea, guanidine hydrochloride) as the

perturbation, transition state locations can be calculated from an analysis of the V-shaped folding relaxation rate vs. denaturant concentration plot, also known as “chevron plot.” The Tanford  $\beta_T$  value from this analysis is an indicator of the relative compactness of the folding transition on the reaction coordinate in terms of solvent accessible surface area [29]. Using temperature as perturbant by analogy [6, 30, 31], a mutant’s  $\Phi_T$  value ( $\Phi_T = \frac{\partial \Delta G^\ddagger / \partial T}{\partial \Delta G / \partial T} = \frac{\Delta S^\ddagger}{\Delta S}$ ) can be used as a quantitative, entropic reaction coordinate that describes how much the transition state shifts along the reaction coordinate because of the mutation. It is worth emphasizing that the  $\Phi_T$  value reports on the overall changes in entropy (i.e. it also includes changes in protein solvation), not just protein conformational entropy. Because the  $\Phi_T$  value is calculated from two derivatives, it is also sensitive to the quality of the raw data with the best results obtained at temperatures close to the midpoint of unfolding ( $T_m$ ).

We first calculated  $\Phi_T$  values directly by taking the derivatives of the second order Taylor series in Table 1. Some of the quadratic coefficients have larger errors than others, and this results in unphysical values of  $\Phi_T$  (SI Fig. 4A), of the temperature of maximal stability  $T_0$  (where  $\Delta G$  is at a minimum), and of heat capacities. We therefore also analyzed the data by Taylor series expanding the free energy around the temperature of maximal stability using  $\Delta G = \Delta G_0 + \Delta G^{(2)}(T-T_0)^2$ . This “ $\Phi_T T_0$ -fit” yields essentially the same  $\Phi_M$  values as the Taylor expansion about  $T_m$  in Table 1 (SI Fig. 4B), and  $\Phi_T$  values with more realistic  $T_0$  for all proteins, so we opt to discuss the “ $\Phi_T T_m$ -fit” throughout this paper. For completeness, we summarize the connection between the Taylor expansion and the common Gibbs-Helmholtz expansion (in terms of the more physical parameters  $\Delta H_0$ ,  $\Delta S_0$  and  $\Delta C_p$ ) in the SI, and provide a table of heat capacities (SI Table 4).

Mutations N30A, T29G, I28N/T29G, S32s and W11F had  $\Phi_T$  values  $> 0.7$  (Fig. 3, dotted horizontal line), which we chose as a reasonable cut-off for distinguishing between conservative and perturbing mutants because the  $\Phi_M$  values of mutants W11F, T29G and I28N/T29G either stand-out as clear outliers or are not cross-validated by other mutants (Fig. 2B). In these mutants, the transition state shifts closer to the native state such that their  $\Phi_M$  values are no

longer reliable indicators of the unperturbed “wild type” transition state ensemble, and thus must be excluded from consensus  $\Phi_M$  analysis. Excluding the abovementioned 5 outliers, the remaining mutants fall within a 25 % interval around the average  $\Phi_T$  value of 0.50 (Fig. 3, horizontal dashed line). Loop 2 mutants in general tend to have higher  $\Phi_T$  values, indicative that loop 2 can compete with loop 1 for becoming rate-limiting at higher temperatures.

The  $\pm 0.2$  spread in the transition state locations as quantified by  $\Phi_T$  is similar to that reported for the FBP28 WW domain, analyzed using Tanford’s  $\beta_T$  value [32]. Even though the individual  $\Phi_T$  values were measured with high precision (error in  $\Phi_T \sim 0.02$ ), the systematic error in  $\Phi_T$  may be substantially larger. This is best seen when we compare the  $\Phi_T$  values of multiple mutations for one residue. Mutants R21A and R21H have very similar  $\Phi_M$  values (0.95 and 0.89) and essentially identical  $\Phi_T$  values (0.44 and 0.45), while mutants R14A, R14L and R14F also have similar  $\Phi_M$  values, but their  $\Phi_T$  values that span 25 %.

The most dramatic shift in  $\Phi_T$  is found for the I28N/T29G mutant, whose large  $\Phi_M$  value ( $0.96 \pm 0.02$ ) also poorly agrees with other loop 2 mutants (Fig. 2B, Table 1). The double mutation I28N/R29G replaces the central two residues of loop 2 with a sequence that has a strong propensity to fold into a tight type-I’ turn, suggesting that loop 2 is particularly prone to mutations that introduce residues that have a low propensity to adopt the helical  $\alpha_R\text{-}\alpha_R\text{-}\alpha_R\text{-}\alpha_L$  backbone conformation that is required to form loop 2. Indeed, the statistically preferred residues at position 29 are Ser and Thr, and at position 30, Arg, Lys, Gly or Asn. Glycines (position 29) and alanines (position 30) are rare, or not found at all among WW domains.

For mutant W11F, the shift in  $\Phi_T$  is accompanied by a very large  $\Phi_M$  value that clearly stands out as a outlier from the mutant pool (Fig. 2A), while the perturbing effect (shift in  $\Phi_T$ ) seen for loop 2 mutants T29G, I28N/T29G, N30A and S32s results in more subtle abnormalities in  $\Phi_M$  that are more difficult to identify by merely looking at the context-dependent  $\Phi_M$  values alone (SI Fig. 5). A third class of mutants (e.g. P8A, S16A, V22A and Y24W) shows clear outlier  $\Phi_M$  values, but normal  $\Phi_T$  values.

#### 4. High-resolution mapping of the folding transition state of hPin1 WW

##### General features of the transition state

Our approach for mapping the folding transition state of hPin1 WW was to pick the most conservative mutant set with  $\Phi_M$  values that were not outliers, based on cross-validation by multiple mutations, sequence neighbors, and backbone hydrogen bond neighbors, and whose  $\Phi_T$  values indicate no excessive shift of the transition state. Thirty-nine mutants (34 side chain and 5 backbone hydrogen bond variants) fulfill these criteria and form a consensus set for transition state analysis (Fig. 4A, Table 2). Except for S19G and I28V, all mutants had  $\Delta\Delta G_f > 2$  kJ/mol, close to or above the empirical cutoff ( $> 2.50$  kJ/mol) for reliable  $\Phi_M$  analysis [33], and except for mutants I28A and E35Q/A, statistical errors in  $\Phi_M$  were small.

Several residues (L7, E12, R14, R21, Y23, F25, I28, T29) in hPin1 WW were probed by more than one side chain mutation. For these residues, we can calculate more robust (and more representative) error-weighted average  $\Phi_M$  values from the side chain  $\Phi_M$  values of individual mutations (Table 2). Mapping the (error-weighted average) side chain  $\Phi_M$  values onto the  $C_\alpha$ -backbone of the folded protein reveals that loop 1 (S16-R21) is substantially more structured in the transition state than loop 2 (H27-N30) and hydrophobic cluster 1 (Fig. 4B).

The (error weighted) average side chain  $\Phi_M$  plot is a smooth function of sequence (Fig. 5A, solid red line), indicating that the formation of transition state structure is governed mainly by local interactions. Even without the outlier mutants S16A/T, a peak at loop 1 is obvious (see SI Fig. 5 for an extended plot, including outliers). While hydrophobic cluster 1 contacts (probed by L7V/A, G10 and Y24F) are essential for hPin1 WW stability, their contribution to the folding rate is small, and folding of hPin1 WW is rate-controlled by the loop 1 substructure that contributes only slightly to thermodynamic stability. The high side chain  $\Phi_M$  value of the C-terminal E35, although corroborated by two mutants (E35A/Q), may not truly report on transition state structure. E35 is a charged residue and solvent-exposed in the folded protein. Except for

mutant S16A, we find good agreement between the  $\Phi_M$  values of individual Ala mutants and the consensus average  $\Phi_M$  value (SI Fig. 5).

### **Correlation between native-state disorder and non-classical $\Phi_M$ -values in loop 1**

Here we propose the hypothesis that  $\Phi_M$  values  $>1$  in loop 1 (see section 2) are due to native-state backbone dynamics. An NMR-solution structure of the apo-form of the isolated WW domain implies that loop 1 is intrinsically dynamic [34] (SI Fig. 3), and this dynamic nature appears to be preserved in the high-resolution X-ray structure (1.35 Å) of hPin1 WW in the context of the full-length hPin1 rotamase (Fig. 5B). Except for M15A in  $\beta$  strand 1, all mutations that yield non-classical  $\Phi_M$  values  $> 1$  mutate residues that map onto the intrinsically more disordered loop 1 region, and the concordance between the average consensus  $\Phi_M$  values (Fig. 5A) and the thermal B factors (a convenient measure for native-state conformational disorder) (Fig. 5C) is striking. The reasonable correlation between the local disorder of a loop 1 residue and the magnitude of its  $\Phi_M$  value (Fig. 5D) suggests that the  $\Phi_M$  values in loop 1 are shifted upward further, from values near 1 that are indicative of the importance of loop 1 in the transition state, to even larger values indicative of native state disorder. A more disordered loop 1 may better accommodate mutations that change backbone and sidechain entropy or perturb backbone hydrogen bonds, and thus yields a lower  $\Delta\Delta G_f$  (and a higher  $\Phi_M$  value), if at the same time the transition state is more sensitive to such mutations because other robust structure (e.g. hydrophobic core 1) have not yet formed.

### **Correlation between side chain and backbone hydrogen bond $\Phi_M$ values**

Hydrophobic cluster 2 (R14-Y23-F25) that stabilizes the N-terminal  $\beta$ -hairpin is loosely formed in the transition state, making an average of 73 % of its native contacts in the transition state (R14 = 77 %, Y23 = 72 %, F25 = 69 %, each calculated from the error-weighted average  $\Phi_M$ , Table 2). The  $\Phi_M$  value of mutant K13k that weakens the E12-F25 backbone hydrogen bond ( $0.80 \pm 0.02$ ) agrees well with the side chain  $\Phi_M$  values of hydrophobic core 2 that protects the hydrogen bond from solvent in native hPin1 WW, suggesting that the E12-F25 backbone hydrogen bond and hydrophobic cluster 2 form cooperatively in the folding transition state.

To test whether this correlation between backbone hydrogen bond and side chain  $\Phi_M$  values generally holds for hPin1 WW, it is helpful to compare the backbone and side chain  $\Phi_M$  values at the level of individual residues. We thus assign the  $\Phi_M$  value of a perturbed backbone hydrogen bond to the two residues that form such a bond, not the residue that is mutated to perturb the hydrogen bond (as done in a previous study [16]). For example, mutation S16s eliminates the S16-R21 backbone hydrogen bond by replacing the amide moiety of the M15-S16 backbone peptide bond that acts as a hydrogen bond donor to form the backbone hydrogen bond with the carbonyl moiety of residue R21 with an ester moiety that cannot engage in backbone hydrogen bond formation (Fig. 1B). Here, we assign the  $\Phi_M$  of the S16s mutant to both residue S16 and R21. Likewise, mutation K13k perturbs, but does not eliminate, the backbone hydrogen bond between residues E12 and F25, by weakening the hydrogen bond acceptor (backbone carbonyl) of E12 (Fig. 1B). Here, however, it would be more correct to assign the  $\Phi_M$  of K13k not to residue K13 but to residues E12 and F25 that form the backbone H, even though formally, the amide-moiety of residue K13 is mutated.

Overall, we find good agreement between the “residue-assigned” backbone  $\Phi_M$  values (Fig. 5A, filled blue circles) and the  $\Phi_M$  values from classical side chain mutation (Fig. 5A, filled red circles), in particular within the hairpin 2 region (Table 2). As the strength of a hydrogen bond is strongly dependent on the distance between the hydrogen bond donor (backbone amide) and hydrogen bond acceptor (backbone carbonyl), even fractional backbone hydrogen bond  $\Phi_M$  values of  $\sim 0.5$  imply that loop 2 is highly compact or that the measured fractional  $\Phi_M$  values within hairpin 2 represent ensemble averages with about 50 % of the molecules having hairpin 2 fully formed in the transition state ensemble ( $\Phi_M \sim 1$ ), while in the other half of molecules hairpin 2 is disordered ( $\Phi_M \sim 0$ ). Such a scenario has been predicted in less extreme form from Markov-State-modeling of hPin1 WW folding [35-37].

The poor agreement between the side chain and backbone  $\Phi_M$  values calculated for residue E12 probably stem from the removal of a solvent-exposed charged residue by mutations E12A/Q. Long-range electrostatic effects may play a role instead of just local contacts.

### Variation of transition state structure with temperature

Probing the folding kinetics not just at a single temperature, but over a wider range of temperatures (here, 50, 55 and 60 °C), reveals the robustness of the transition state ensemble against thermodynamic stress. Folding studies at various temperatures also identify ‘borderline’ mutations that perturb the folding mechanism under increased thermal stress, but whose disruptive nature might escape detection under more favorable folding conditions.

On average, the  $\Phi_M$  values increase by 0.07 units (Fig. 6A) and the  $\Phi_T$  value increases by 0.15 units (Fig. 6B) upon raising the temperature from 50 to 60 °C (for data, see SI Table 1, 2). This suggests that the folding transition state becomes more structured and native-like at higher temperature, and the transition state ensemble shifts along the reaction coordinate closer to the native state, in agreement with Hammond’s postulate [38].

A plot of  $\Phi_M(60^\circ\text{C})/\Phi_M(50^\circ\text{C})$  vs. sequence in Fig. 6C reveals that structure within hairpin 1 (residues 12-25) at best changes only weakly with temperature. In contrast the loop 2 region (residues 27-30), the third  $\beta$  strand (residues 31-34) and hydrophobic core 1 (probed by L7A and L7V) increase by a larger margin and beyond experimental uncertainty. The absolute changes in  $\Phi_M$  are, however, rather small such that hairpin 1 still dominates transition state structure at higher temperatures. The Ala mutant W34A may show unusual temperature tuning (although it has a large error bar in Fig. 6C), and we speculate on a possible origin in the SI.

### Average fraction of native contacts and its temperature dependence

For the set of consensus mutants depicted in Fig. 4A, we calculate an average  $\Phi_M$  value of  $0.68 \pm 0.04$  at 55 °C, which is higher than the overall average  $\Phi_T$  value (0.50 at 55 °C, excluding the 5 outliers discussed in sections 3 and 4). Mutants with a higher slope of  $\Delta G$  vs.  $T$  (folding

cooperativity) have a higher melting temperature ( $T_m$ ) (Fig. 7A, where  $\Delta G=0$  at  $T=T_m$  for all mutants). The average slope is +0.0017 kJ/mole/K, indicative of a negative folding entropy  $\Delta S=-(\partial\Delta G/\partial T)$ , and increases by about 0.1 kJ/mole/K over the 35-60 °C range of melting temperatures. The size-dependence of  $\Delta S$  for folding has been discussed in the literature [39, 40]. From the temperature dependence of the folding barrier on protein stability (Fig. 7B), we calculate a slope  $(\partial\Delta G^\ddagger/\partial T) \approx 0.0024$  kJ/mole/K (0.0028 for all mutants listed in Table 1). The ratio of the two slopes (activated/ground) is  $\sim 0.70$  (0.63 for all mutants listed in Table 1). This value is also higher than the average  $\Phi_T$  value of 0.50, and suggests that there is a significant unfolding cooperativity effect in the folding transition state, although not as high as the unfolding cooperativity seen in the native protein. The  $\Phi_T$  value thus seems to slightly overestimate the distance of the transition state to the native state.

## 5. $\Phi_M$ analysis of loop 1 insertion and deletion mutants

### Mutant design and structural analysis

We recently designed and biophysically characterized several hPin 1 WW variants in which the wild type loop 1 sequence is replaced by either a 5-residue type-I G-bulge turn (the preferred loop type in WW domains) or tighter, 4-residue type-I' turns that are not found among WW domains [7] (Fig. 8A).

The X-ray structures of the most stable type-I G-bulge variant (var1, or FiP, loop sequence: SADGR) and the most stable type-I' turn variant (var3, loop sequence: SNGR) have been solved at 1.90 and 1.50 Å resolution, respectively. Both variants essentially superimpose with the wild type structure (1.35 Å resolution), except for the redesigned loop 1 region (Fig. 8B). The thermal B factors of the FiP variant are consistently lower than that of wild type hPin 1 WW, while those of var3 are higher (SI Fig. 6). While the difference in the absolute values of the thermal B factors may result from different crystal packings, we note that turn 1 in the X-ray structure of FiP appears to be conformationally rigid, consistent with NMR-solution data of the same turn in its natural FBP28 WW context (SI Fig.3). The 4-residue type-I' turn of variant 3 shows a relative maximum in the B factor similar that of loop 1 in wild type hPin1 WW, suggesting that the type-

l' turn, although stabilizing and hastening hPin1 WW folding, is conformationally flexible in the folded protein.

### Group $\Phi_M$ analysis and $\Phi_M$ vs. $\Delta\Delta G_f$ correlation

At 60 °C, and using wild type hPin1 WW as the reference protein, we calculate  $\Phi_M$  values of  $0.92 \pm 0.01$  for FiP and  $0.91 \pm 0.01$  for the related variant 2. Both  $\Phi_M$  values are cross-validated by the  $\Phi_M$  value of variant 2 calculated with FiP as “pseudo wild type” reference ( $0.94 \pm 0.05$ ) (Fig. 8D), demonstrating that  $\Phi_M$  analysis is surprisingly robust towards more severe sequence manipulations that simultaneously alter sequence and local chain topology. The  $\Phi_M$  values of FiP and related variant 2 also agree well with the  $\Phi_M$  values of mutants R21A, R21H and S16s ( $\Phi_M = 0.83$ - $0.97$ ) measured in the wild type loop context (Fig. 8C, D). This correlation is remarkable in that the mutants differ by up to 15 kJ/mole in stability. It further implies that in the strictly sequential folding model (loop 1 first, then loop 2) proposed for FiP by Shaw et al., the energy barrier of the second transition (loop 2 nucleation) must be sufficiently small for FiP-variant 2 to yield a  $\Phi_M$  value =  $0.94 \pm 0.05$  (SI Fig. 7A). The GTT variant of FiP with an optimized loop 2 structure, however, significantly accelerates FiP folding (by a factor of three), suggesting that loop 2 formation in FiP is associated with a non-negligible barrier and rate-limiting for folding (SI Fig. 7B). Both observations are contradictory and difficult to reconcile in the framework of a sequential model, but perfectly compatible with a simple two-state mechanism, as in the latter case, stabilizing loop 1 and loop 2 mutations may additively lower the (single) transition barrier (SI Fig. 7C).

Type-l' turn variants also hasten wild type hPin1 WW folding, but by a smaller margin than in FiP. In contrast, the two Gly insertion variants 6 and 7 (both less stable than wild type) slow down folding, presumably because of an increased entropic penalty to form the longer 7- or 8-residue loop 1 substructure. All four variants yield  $\Phi_M$  values greater than 1, similar in magnitude to the  $\Phi_M$  values of wild type mutants S16G, S18G, S18G/S19G and G20A (Fig. 8D). As for wild type hPin1 WW (Fig. 5), increased local backbone dynamics around the type-l' turn may cause the already high  $\Phi_M$  values to fall outside the classical range.

### Hypothetical hybrid $\Phi_M$ -map of FiP and comparison with MD-simulations

$\Phi_M$  values are determined experimentally as a ratio of logarithms of rates to logarithms of equilibrium constants. This can be simulated directly by computation (using long trajectories or multiple shorter trajectories with Markov analysis to obtain rate and equilibrium constants), or it can be done by examining structure near the transition state (which has a  $P_{\text{fold}} \approx 1/2$  folding probability) and comparing with native structure (based on native contacts). In principle, the kinetic/energetic method is the more direct comparison, but structural information may have smaller error bars than energy information, so there is a tradeoff between the two approaches. Extensive data sets such as those in the present paper should become amenable to both approaches in the next few years, to test the merits of the structural vs. energetic approach to simulated  $\Phi_M$  values in detail. Here we present a brief comparison of our results, adapted to the FiP modification (see loop mutants in Table 1 for example) of WW domain, and comparing with ref. [14], which presents both structure-based (native side chain contacts) and energy based (long trajectory kinetics)  $\Phi_M$  values. In the case of [14], the difference between experiment and the two computational approaches still exceeds the difference between the computations, so it appears that force field errors currently still dominate over errors caused by the structural approximation.

We assume that replacing the wild type hPin1 WW loop with the FiP loop 1 sequence only affects the local loop 1 energetics. This assumption is justified by the smooth dependence of  $\Phi_M$  on sequence, and by the nearly superimposable loop 2 and hydrophobic core 1 substructures of FiP and wild type hPin1 WW (Fig. 8B). A hypothetical “hybrid”  $\Phi_M$ -map can be rendered for the ultrafast-folding FiP variant by combining the loop 1  $\Phi_M$  value of FiP variant 2 ( $0.94 \pm 0.05$ , measured with FiP as the “pseudo wild type” reference) with the non-loop 1  $\Phi_M$  values obtained with wild type hPin1 WW (Fig. 9, red symbols and solid red line).

For loop 1 and its immediate sequence neighbors, our putative “hybrid”  $\Phi_M$  map (60 °C) agrees well with the simulated  $\Phi_M$  map calculated at slightly higher temperature (75 °C) [14]. This

reinforces our hypothesis (previous paragraph) that replacing loop 1 in wild type hPin1 WW with more stable sequences hastens folding without changing the folding mechanism - either loop type is substantially (or fully) formed in the folding transition state. The  $\Phi_M$  values within the loop 2 region, however, do not agree very well. Here, the experimental  $\Phi_M$  values clearly suggest more structure within hairpin 2 than the MD-simulation [14]. As loop 2 slightly gains structure with temperature this discrepancy should be even more pronounced at 75 °C (the temperature used for MD-simulations).

Shaw *et al.* argue that the folding mechanism of FiP is a direct consequence of the difference in the thermal stability of the N- and C-terminal hairpins. Although the isolated hairpins fold about one order of magnitude faster than full-length FiP and at similar rates in simulations, hairpin 1 with the optimized loop 1 sequence is significantly more stable (25 % folded hairpin at equilibrium) than hairpin 2 (4 % folded hairpin at equilibrium), such that loop 1 nucleation is expected to kinetically outperform loop 2 nucleation. Although plausible, this model does not take into account the aforementioned significant (approximately 3-fold) increase in the folding rate that is seen experimentally with the GTT-FiP variant.

In hPin1 WW with the unstable and intrinsically flexible 6-residue loop 1 sequence, isolated hairpin 1 is expected to be much less stable, perhaps even less stable than isolated hairpin 2. This would open up three possible folding scenarios:

With both hairpins being similarly unstable, folding could occur through parallel pathways nucleated by either loop substructure (scenario 1), as predicted from Markov-state-modeling of hPin1 WW folding. In this case, the experimentally measured  $\Phi_M$  values for the loop 1 and loop 2 regions would directly describe the relative flux along either pathway. In the simplest, and most extreme case, the hairpin whose loop segment nucleates folding is fully formed in the transition state ( $\Phi_M \sim 1$ ) while the other hairpin is completely unstructured ( $\Phi_M \sim 0$ ). For loop 2, we find average  $\Phi_M$  values of  $\sim 0.60$  at 60 °C. Therefore, if that extreme model applied, one would expect  $\Phi_M$  values of only  $\sim 0.40$  for loop 1, which is clearly not what we observe

experimentally (average  $\Phi_M > 0.9$  at 60 °C).

Alternatively, both loop substructures may fluctuate between an open and a closed state, although not necessarily a native-like state, however a native-like N-terminal hairpin is mandatory for barrier-limited folding into the native state (scenario 2). In this model, loop 1 residues will by necessity yield the highest  $\Phi_M$  values, while the loop 2  $\Phi_M$  values will be reporters about the equilibrium ratio of the open and closed hairpin 2 conformations before their interaction with the structured N-terminal hairpin occurs. As loop 2 formation could either occur before or after loop 1/hairpin 1 formation, hairpin 1 would “catalyze” the final transition of hairpin 2 from the closed to the native state. This folding model is unlikely for wild type hPin1 WW domain because an increase in temperature should shift the loop 2 equilibrium towards the open (less structured) conformation, so the loop 2  $\Phi_M$  should decrease with temperature, rather than (slightly) increase. It may, however, become a dominant mechanism in fast-folding WW domains such as FiP.

The most likely folding model for hPin1 WW thus remains a two-state folding mechanism, in which folding and docking of the hairpins occurs in a concerted fashion. The measured  $\Phi_M$  values would then imply that the N-terminal hairpin is mainly formed in the transition state, while the second hairpin and the hydrophobic core are in the process of being formed in the transition state. Two-state folding of not only wild type hPin1 WW, but also the FiP variant, would also better explain why certain FiP variants such as FiP-GTT with stabilizing mutations within loop 2 and  $\beta$  strand 3 speed up its folding despite high  $\Phi_M$  values near unity in the hairpin 1 turn region.

## Conclusions

$\Phi_M$ -value analysis can provide valuable information about the structure of folding transition states by correlating changes in mutationally induced stability and folding kinetics. In its simplest manifestation,  $\Phi_M$ -value analysis can be affected by probe perturbation of the folding mechanism, and by a trickle-down effect of mutations that lowers the structural resolution.

Such trickle down effects can arise for instance from native state flexibility, or from solvent interactions that do not report on genuine structure *per se*.

Here we present a comprehensive  $\Phi_M$ -value analysis with horizontal (sequence), vertical (multiple mutations at a single site) and chemical depth (side chain and “residue-assigned” backbone hydrogen bond mutations) to identify reliable mutations that can act as probes of the folding mechanism. The “conservatism” of mutations with respect to the folding mechanism is ascertained by multiple side chain substitutions at the same site (L7, E12, R14, S16, Y23, Y24, F25, I28 and T29), verification of individual  $\Phi_M$  values by cross- $\beta$  strand neighbors (M15 vs. V22, E12 vs. F25), residue assigned  $\Phi_M$  values from backbone hydrogen bond mutagenesis (e.g. S16A/G/T vs. S16s, N26D vs. H27h) or immediate sequence neighbors (R21-V22-Y23 series), and temperature tuning (outliers in  $\Phi_T$ ).

For some residues (R14, T29),  $\Phi_M$  values calculated from non-conservative mutations agree well with  $\Phi_M$  values calculated from more conservative and structurally less perturbative mutations, while other mutations yield  $\Phi_M$  values that primarily report on the energetics of polar or charged residues with solvent (e.g. Y23F, E12A/Q, E35A/Q). Another subclass of mutations that target the flexible loop 1 substructure of hPin1 WW (S16G, R17r, S19G, S18G/S19G, G20A) yield  $\Phi_M$  values that lie clearly outside the classical range ( $\Phi_M > 1$ ). Based on the correlation with X-ray B factors, their high  $\Phi_M$  values result at least in part from increased local backbone dynamics in the native state.

Although Ala mutations overall appear to be reliable reporters of transition state structure, as often assumed in the literature, we also identify clear outliers (P8A, S16A and V22A). Another Ala-mutant (W34A) shows an unusual dependence on temperature tuning. Its  $\Phi_M$  value decreases with temperature, suggesting that the smaller Ala residue perturbs non-native interactions that are stable at low temperature, yet nevertheless speed up folding.

Aside from obvious mutant outliers that can be easily identified by cross-validating their  $\Phi_M$  values with different mutants at the same sequence location, another subset of mutants perturb transition state structure and shift the transition state ensemble to a more native-like ensemble state, as evidenced by large  $\Phi_T$  values for such mutations. Four of the five mutants that shift the transition state position in Fig. 5 map to the loop 2 region or immediately flanking residues. Although not dominating transition state structure, the wild type sequence of loop 2 can be perturbed sufficiently to affect folding rates. The ease with which the folding mechanism of the hPin1 WW domain can be changed by what appears to be subtle sequence modifications or perturbations of intermolecular forces (e.g. weakening a single, partially solvent-exposed backbone hydrogen bond as in amide-to-ester mutant S32s) argues against two-state folding with a well-defined, robust and narrow transition state and suggests a more complex, multidimensional energy surface with additional local extrema waiting to become rate limiting for folding, as shown experimentally and computationally for the FBP28 WW domain [4, 41]. The hPin1 WW domain is thus an apparent two-state folder, but not by a wide margin.

Using a more expanded set of consensus mutants, a detailed map of the folding transition state was generated that now covers 76 % of the hPin1 sequence (previous coverage: 50 %). Many of our earlier findings are supported in the present study, but some interpretations need to be modified or revisited. Loop 2 and  $\beta$  strand 3, which define the C-terminal hairpin in folded hPin 1 WW, appear to be more structured in the transition state than thought previously, and the discrepancy in the backbone and side chain  $\Phi_M$  values within the loop 1 substructure can now be attributed to local backbone disorder in the folded protein, rather than a genuine variation in backbone and side chain structure. In fact, by assigning backbone hydrogen bond to the two residues that constitute the bond, we found good agreement between the  $\Phi_M$  values measured by side chain and backbone hydrogen bond perturbation for most positions.

The mutants with a thermodynamically and kinetically optimized loop 1 substructure agree well with the native-like  $\Phi_M$  values of the highly destabilized loop 1 variants R21A/H and S16s mutants that perturb the 6-residue wild type hPin1 WW loop. Clearly, in both wild type hPin1

and the redesigned variants, the tip of the loop/turn is fully developed in the transition state. These observations and the fact that stabilizing loop 2 in the already fast folding FiP domain further speeds up folding by a factor of 3 are difficult to reconcile in a truly sequential (framework) model for folding, making a simple two-state folding mechanism more likely. Alternatively, as suggested by some simulations [35, 42 ] and experiments [43] of fast-folding WW domains, loop 2 could actually form before or after loop 1, or fluctuate between folded and unfolded conformations before loop 1 forms, while loop 1 remains rate-limiting due to its larger activation barrier. Additional experiments with mutations targeting loop 2 in FiP are needed to further discriminate between these alternatives.

## **Materials and Methods**

### **Nomenclature**

Residues of the hPin1 WW domain are abbreviated by a single capital letter, followed by the number of the residue in the sequence (e.g. W11). Amino acids are also abbreviated using the standard three letter code (e.g. Trp for tryptophan). Classical side chain mutants are indicated by single letter code (e.g. W11F), with the first and second letters representing the wild type and replacing residue, respectively, and the number indicates the sequence position. Non-classical backbone hydrogen bond mutations are also designated by single letter code. The first letter represents the mutated residue, and the same letter in small capitals is used for the replacing residue (e.g. S16s) to distinguish a non-classical amide-to-ester mutation from their classical counterparts.

### **Protein expression and sample preparation**

The wild type hPin1 WW domain and mutants thereof with classical side chain mutations were prepared recombinantly, as described in detail in another publication [10]. hPin1 WW variants with amide-to-ester mutations were synthesized chemically, as described in detail in [16]. Protein identity and purity was ascertained by electrospray mass spectrometry, SDS-PAGE, and reversed-phase HPLC chromatography.

### Experimental procedures

Equilibrium unfolding of hPin1 WW was monitored by far-UV spectroscopy at 229 nm as described in detail in [10]. Unfolding transitions were analyzed by using a two-state model, where the folding free energy  $\Delta G_f$  is expressed by a quadratic Taylor series approximation:  $\Delta G_f(T) = \Delta G_f^{(1)}(T_m)(T - T_m) + \Delta G_f^{(2)}(T_m)(T - T_m)^2$ . The two coefficients  $\Delta G_f^{(i)}(T_m)$ ,  $i=1 \dots 2$ , represent the temperature-dependent free energy of folding, and  $T_m$  is the nominal midpoint of thermal denaturation ( $\Delta G_f(T_m) = 0$ ). The inclusion of the quadratic term was necessary to fit the data of most mutants within experimental uncertainty. For selected mutants, the transition was also analyzed by expressing  $\Delta G_f(T)$  in terms of a constant heat capacity formula. As shown previously for the hYap65 WW domain, both procedures yield nearly identical results [31].

Laser temperature jumps around the protein's melting temperature were measured for each mutant as described in detail elsewhere [44, 45]. Briefly, a 10 ns Nd:YAG pulse Raman-shifted in H<sub>2</sub> heated the sample solution by  $\sim 5$ -10 °C, inducing kinetic relaxation of the WW domain to the new thermal equilibrium. 285 nm UV pulses, spaced 1 ns apart from a frequency-tripled, mode-locked titanium:sapphire laser, excited tryptophan fluorescence in the hPin1 WW domain. Fluorescence emission was digitized in 0.5 ns time steps by a miniature photomultiplier tube with a 0.9 ns full-width-half-maximum response time. The sequence of fluorescence decays  $f(t)$  was fitted within measurement uncertainty by the linear combination  $a_1 f_1(t) + a_2 f_2(t)$  of decays just before and 0.5 ms after the T-jump. The normalized fraction  $f(t) = a_1 / (a_1 + a_2)$  from  $t \approx 2 \mu\text{s}$  to  $t = 0.5 \text{ ms}$  was fitted to a single exponential decay  $\exp[-k_{\text{obs}} t]$  where  $k_{\text{obs}} = k_f + k_u$ . Thus the signal extraction and data analysis are consistently two-state.

The observed relaxation rate coefficient was combined with the equilibrium constant  $K_{\text{eq}}$  to compute the forward reaction rate coefficient  $k_f = k_{\text{obs}} K_{\text{eq}} / (1 + K_{\text{eq}})$ .  $k_f$  was measured for several temperatures (typically around 10) below and above  $T_m$ , and  $\Delta G_f^\ddagger(T)$  was determined as a function of temperature using the relationship  $k_f = A^\ddagger \exp(-\Delta G_f^\ddagger(T)/RT)$  with the quadratic Taylor approximation  $\Delta G_f^\ddagger(T) = \Delta G_f^{\ddagger(0)}(T_m) + \Delta G_f^{\ddagger(1)}(T_m)(T - T_m) + \Delta G_f^{\ddagger(2)}(T_m)(T - T_m)^2$ , as well as expansions about the temperature of maximal stability ( $T_0$ ), or the Gibbs-Helmholtz formula (see SI). The

three coefficients  $\Delta G_f^{\dagger(i)}$ ,  $i=0\text{--}2$ , represent the temperature-dependent activation barrier. The frequency of activation  $A^\dagger$  was fixed at  $500\text{ ns}^{-1}$ , near the lower end of estimates of the folding speed limit [1], and the two coefficients  $\Delta G_f^{\dagger(1)}(T_m)$  and  $\Delta G_f^{\dagger(2)}(T_m)$  also incorporate some effects of temperature-dependent solvent friction. Because previous  $\Phi_M$  analyses utilized a faster *ad hoc* frequency of  $50\text{ ns}^{-1}$ , the  $\Phi_M$  values of published mutants are shifted by a small constant from the recalculated values of these mutants in this study. Least squares fitting was carried out using IGOR Pro (Wavemetrics). Protein visualization was rendered using Pymol and Weblab viewer software packages (Accelrys, San Diego) [46].

## Acknowledgments

This work was supported by R01 GM 93318 (M.G.) and GM051105 (J.W.K.). M.J. and J.W.K. thank Gina Dendle (The Scripps Research Institute, La Jolla, CA) for expert assistance in hPin1 WW mutant expression and purification. M.J. was supported in part by fellowships from the German Research Council (DFG) and the La Jolla Interfaces in Science (LJIS) training program while this work was carried out.

**Author Contributions.** M.J., J.W.K. and M.G. designed research; M.J. and H.N. performed research; K.D., M.J., H.N. and M.G. analyzed data; K.D., M.J., H.N., J.W.K. and M.G. contributed data analysis tools, K.D., M.J. and M.G. wrote the paper. All authors read and approved this article for publication.

**Conflict of Interest Statement.** The authors declare no conflict of interest.

**Keywords:** Protein folding; WW domain;  $\Phi$ -value analysis; folding transition state; laser T-jump

**Abbreviations used:** B factor, thermal B factor, a measure for backbone dynamics from X-ray crystal structures; FBP28 WW, WW domain (residues 1-37) derived from mouse formin binding protein 28; FiP, hPin1 WW variant in which the wild type loop 1 sequence (SRSSGR) is replaced by a sequence that folds into a type-I G-bulge turn (sequence: SADGR); FiP-GTT, stabilized FiP variant with the triple mutation N30G/A31T/S32T that hasten folding of FiP threefold at the thermal midpoint of unfolding; hPin1 WW, WW domain (residues 6-39) derived from human *cis/trans*-isomerase Pin1; hYap65 WW, WW domain (residues 1-45) derived from human Yes-associated protein 65; MD-simulation, molecular dynamics simulation; NMR, nuclear magnetic resonance;  $\Phi_M$ , mutational phi value, an indicator for structure in the folding transition state;  $\Phi_T$ , temperature-dependent phi value, a parameter for mapping the position of the folding transition state along an entropic reaction coordinate.

## References

- [1] J. Kubelka, J. Hofrichter, W.A. Eaton, The protein folding 'speed limit', *Curr. Opin. Struct. Biol.* 14 (2004) 76-88.
- [2] R.D. Schaeffer, A. Fersht, V. Daggett, Combining experiment and simulation in protein folding: closing the gap for small model systems, *Curr. Opin. Struct. Biol.* 18 (2008) 4-9.
- [3] F. Cecconi, C. Guardiani, R. Livi, Testing simplified proteins models of the hPin1 WW domain, *Biophys. J.* 91 (2006) 694-704.
- [4] H. Nguyen, M. Jäger, A. Moretto, M. Gruebele, J.W. Kelly, Tuning the free-energy landscape of a WW domain by temperature, mutation, and truncation, *Proc. Natl. Acad. Sci. U. S. A.* 100 (2003) 3948-3953.
- [5] H.I. Chen, M. Sudol, The WW domain of Yes-associated protein binds a proline-rich ligand that differs from the consensus established for Src homology 3-binding modules, *Proc. Natl. Acad. Sci. U. S. A.* 92 (1995) 7819-7823.
- [6] M. Jager, H. Nguyen, J.C. Crane, J.W. Kelly, M. Gruebele, The folding mechanism of a beta-sheet: The WW domain, *J. Mol. Biol.* 311 (2001) 373-393.

- [7] M. Jäger, Y. Zhang, J. Bieschke, H. Nguyen, M. Dendle, M.E. Bowman, et al., Structure–function–folding relationship in a WW domain, *Proc. Natl. Acad. Sci. U. S. A.* 103 (2006) 10648-10653.
- [8] S. Gianni, C. Camilloni, R. Giri, A. Toto, D. Bonetti, A. Morrone, et al., Understanding the frustration arising from the competition between function, misfolding, and aggregation in a globular protein, *Proc. Natl. Acad. Sci. U. S. A.* 111 (2014) 14141-14146.
- [9] S. Piana, K. Sarkar, K. Lindorff-Larsen, M. Guo, M. Gruebele, D.E. Shaw, Computational Design and Experimental Testing of the Fastest-Folding  $\beta$ -Sheet Protein, *J. Mol. Biol.* 405 (2011) 43-48.
- [10] M. Jäger, M. Dendle, J.W. Kelly, Sequence determinants of thermodynamic stability in a WW domain—An all- $\beta$ -sheet protein, *Protein Science : A Publication of the Protein Society* 18 (2009) 1806-1813.
- [11] S. Deechongkit, H. Nguyen, E.T. Powers, P.E. Dawson, M. Gruebele, J.W. Kelly, *Nature* 430 (2004) 101.
- [12] J.G.B. Northey, K.L. Maxwell, A.R. Davidson, Protein Folding Kinetics Beyond the  $\Phi$  Value: Using Multiple Amino Acid Substitutions to Investigate the Structure of the SH3 Domain Folding Transition State, *J. Mol. Biol.* 320 (2002) 389-402.
- [13] K. Lindorff-Larsen, S. Piana, R.O. Dror, D.E. Shaw, How Fast-Folding Proteins Fold, *Science* 334 (2011) 517-520.
- [14] D.E. Shaw, P. Maragakis, K. Lindorff-Larsen, S. Piana, R.O. Dror, M.P. Eastwood, et al., Atomic-Level Characterization of the Structural Dynamics of Proteins, *Science* 330 (2010) 341-346.
- [15] S.V. Krivov, The Free Energy Landscape Analysis of Protein (FIP35) Folding Dynamics, *J. Phys. Chem. B* 115 (2011) 12315-12324.
- [16] S. Deechongkit, P.E. Dawson, J.W. Kelly, Toward Assessing the Position-Dependent Contributions of Backbone Hydrogen Bonding to  $\beta$ -Sheet Folding Thermodynamics Employing Amide-to-Ester Perturbations, *J. Am. Chem. Soc.* 126 (2004) 16762-16771.
- [17] M. Petrovich, A.L. Jonsson, N. Ferguson, V. Daggett, A.R. Fersht, phi-Analysis at the experimental limits: Mechanism of beta-hairpin formation, *J. Mol. Biol.* 360 (2006) 865-881.
- [18] N.R. Guydosh, A.R. Fersht, A Guide to Measuring and Interpreting phi-values, *Protein Folding Handbook* (2005) 445-453.
- [19] T.R. Weikl, Transition States in Protein Folding Kinetics: Modeling  $\Phi$ -Values of Small  $\beta$ -Sheet Proteins, *Biophys. J.* 94 (2008) 929-937.
- [20] M.A. De Los Rios, B.K. Muralidhara, D. Wildes, T.R. Sosnick, S. Marqusee, P. Wittung-Stafshede, et al., On the precision of experimentally determined protein folding rates and  $\phi$ -values, *Protein Science : A Publication of the Protein Society* 15 (2006) 553-563.
- [21] I. Ruczinski, K.W. Plaxco, Some recommendations for the practitioner to improve the precision of experimentally determined protein folding rates and  $\Phi$  values, *Proteins* 74 (2009) 461-474.
- [22] I. Ruczinski, T.R. Sosnick, K.W. Plaxco, Methods for the accurate estimation of confidence intervals on protein folding  $\phi$  - values, *Protein Sci.* 15 (2006) 2257-2264.
- [23] A.N. Naganathan, V. Muñoz, Insights into protein folding mechanisms from large scale analysis of mutational effects, *Proceedings of the National Academy of Sciences* 107 (2010) 8611-8616.
- [24] P. Ferrara, A. Caflisch, Folding simulations of a three-stranded antiparallel beta-sheet peptide., *Proc. Natl. Acad. Sci.* 97 (2000) 10780-10785.
- [25] R. Zhou, G.G. Maisuradze, D. Suñol, T. Todorovski, M.J. Macias, Y. Xiao, et al., Folding kinetics of WW domains with the united residue force field for bridging microscopic motions and experimental measurements, *Proceedings of the National Academy of Sciences* 111 (2014) 18243-18248.

- [26] A.R. Fersht,  $\Phi$  value versus  $\psi$  analysis, *Proc. Natl. Acad. Sci. U. S. A.* 101 (2004) 17327-17328.
- [27] T. Sharpe, A.L. Jonsson, T.J. Rutherford, V. Daggett, A.R. Fersht, The role of the turn in beta-hairpin formation during WW domain folding, *Protein Sci.* 16 (2007) 2233-2239.
- [28] S.L. Lin, A. Zarrine-Afsar, A.R. Davidson, The osmolyte trimethylamine-N-oxide stabilizes the Fyn SH3 domain without altering the structure of its folding transition state, *Protein Sci.* 18 (2009) 526-536.
- [29] J.L. Howland. *Structure and Mechanism in Protein Science. A guide to Enzyme Catalysis and Protein Folding*: Alan Fersht, W.H. Freeman and Company, New York, 1999, 631 pp, ISBN 0-7167-3268-8, \$53.002001.
- [30] J. Ervin, M. Gruebele, Quantifying Protein Folding Transition States with  $\Phi(T)$ , *J. Biol. Phys.* 28 (2002) 115-128.
- [31] J.C. Crane, E.K. Koepf, J.W. Kelly, M. Gruebele, Mapping the transition state of the WW domain  $\beta$ -sheet1, *J. Mol. Biol.* 298 (2000) 283-292.
- [32] C. Tanford, Protein denaturation, *Adv. Protein Chem* 24 (1970) 95.
- [33] A.R. Fersht, S. Sato,  $\Phi$ -Value analysis and the nature of protein-folding transition states, *Proc. Natl. Acad. Sci. U. S. A.* 101 (2004) 7976-7981.
- [34] J.A. Kowalski, K. Liu, J.W. Kelly, NMR solution structure of the isolated Apo Pin1 WW domain: Comparison to the x-ray crystal structures of Pin1, *Biopolymers* 63 (2002) 111-121.
- [35] D.L. Ensign, V.S. Pande, The Fip35 WW Domain Folds with Structural and Mechanistic Heterogeneity in Molecular Dynamics Simulations, *Biophys. J.* 96 (2009) L53-L55.
- [36] F. Noé, C. Schütte, E. Vanden-Eijnden, L. Reich, T.R. Weikl, Constructing the Equilibrium Ensemble of Folding Pathways from Short Off-Equilibrium Simulations, *Proc. Nat. Acad. Sci. USA* 106 (2009) 19011-19016.
- [37] T.J. Lane, G.R. Bowman, K. Beauchamp, V.A. Voelz, V.S. Pande, Markov state model reveals folding and functional dynamics in ultra-long MD trajectories, *J. Am. Chem. Soc.* 133 (2011) 18413-18419.
- [38] G.S. Hammond, A correlation of reaction rates, *J. Am. Chem. Soc.* 77 (1955) 334-338.
- [39] G.P. Brady, K.A. Sharp, Entropy in protein folding and in protein—protein interactions, *Curr. Opin. Struct. Biol.* 7 (1997) 215-221.
- [40] M.S. Li, D.K. Klimov, D. Thirumalai, Finite Size Effects on Thermal Denaturation of Globular Proteins, *Phys. Rev. Lett.* 93 (2004) 268107.
- [41] G.G. Maisuradze, R. Zhou, A. Liwo, Y. Xiao, H.A. Scheraga, Effects of Mutation, Truncation, and Temperature on the Folding Kinetics of a WW Domain, *J. Mol. Biol.* 420 (2012) 350-365.
- [42] S. a Beccara, T. Škrbić, R. Covino, P. Faccioli, Dominant folding pathways of a WW domain, *Proceedings of the National Academy of Sciences* 109 (2012) 2330-2335.
- [43] A.J. Wirth, Y. Liu, M.B. Prigozhin, K. Schulten, M. Gruebele, Comparing Fast Pressure Jump and Temperature Jump Protein Folding Experiments and Simulations, *J. Am. Chem. Soc.* 137 (2015) 7152-7159.
- [44] R.M. Ballew, J. Sabelko, C. Reiner, M. Gruebele, *Rev. Sci. Instrum.* 67 (1996) 3694.
- [45] J. Ervin, J. Sabelko, M. Gruebele, *J. Photochem. Photobiol., B* 54 (2000) 1.
- [46] W.L. DeLano. *The PyMOL Molecular Graphics System*
- [47] M. Jager, Y. Zhang, M.E. Bowman, J.P. Noel, J.W. Kelly. 2F21: human Pin1 Fip mutant. *Worldwide Protein Data Bank*; 2006.

## Figure Captions

**Figure 1: hPin1 WW structure and native state interactions.** (A) Structural cartoon of the hPin1 WW fold, highlighting the two hydrophobic clusters that protrude from either side of the three-stranded  $\beta$  sheet. The individual  $\beta$  strand are color coded blue, while the loop segments and the N- and C-terminal extensions are shown in grey. Side chain contacts that constitute the hydrophobic clusters are shown as van der Waals surfaces. (B)  $C_{\alpha}$ -backbone representation of the three-stranded  $\beta$  sheet region (residues W11-W34), highlighting the ten backbone hydrogen bonds that connect the three  $\beta$  strands and stabilize the 3-stranded  $\beta$  sheet topology. Hydrogen bonds that were perturbed by amine-to-ester mutations for  $\Phi_M$  analysis are labeled in red. Residues are labeled in single letter code and are numbered. (C) Quantitative analysis of a complete Ala-scan, replacing each of the 33 non-Alanine residues individually with Ala. Destabilizations calculated at 55 °C range from near zero to  $\sim 9$  kJ/mole and are mapped onto the  $C_{\alpha}$ -backbone structure of the folded protein. Four Ala-mutants (labeled black) were either completely or significantly unfolded, even at low temperature (4 °C). For these four mutants,  $\Delta\Delta G$  must exceed 9 kJ/mol, but no accurate thermodynamic data can be derived in aqueous buffer without invoking stabilizing co-solvents.

**Figure 2:  $\Phi_M$ -value analysis at 55 °C.** (A) Plot of the  $\Phi_M$  value vs the difference in free energy between wild type and mutant ( $\Delta\Delta G$ , in kJ/mol) for  $\beta$  strand (filled red circles) and hydrophobic cluster 1 mutants (filled black circles). (B) Plot of the  $\Phi_M$  value vs the difference in free energy between wild type and mutant ( $\Delta\Delta G$ , in kJ/mol) of loop 1 (filled blue circles) and loop 2 mutants (filled green circles). Errors in  $\Phi_M$  that exceed the symbol size are shown explicitly. For clarity, individual  $\Phi_M$ -values are labeled with single letter code. Raw data used to render the plots are provided in Table 1.

**Figure 3:  $\Phi_T$  analysis at 55 °C:** Plot of the  $\Phi_T$  value for wild type hPin1 WW and mutants thereof vs the change in free energy ( $\Delta\Delta G$ , in kJ/mol) between wild type and mutant.  $\Phi_T$  values are

calculated using the  $T_0$ -fitting procedure (for details, see SI supporting text 1).  $\Phi_T$  values of side chain and backbone hydrogen bond mutants are color coded red and blue, respectively. Except the obvious five outliers (mutants W11F, T29G, I28N/T29G, N30A, S32s), the  $\Phi_T$  values are within a  $\pm 25\%$  error margin of the average  $\Phi_T$  (0.50, dashed grey horizontal line). The outlier  $\Phi_T$  values ( $> 0.70$ , dotted grey line) are indicative of perturbing mutations that shift the transition state ensemble along the reaction coordinate closer to the native state. Mutational  $\Phi_M$  values calculated from these mutants are no longer reliable indicators of the unperturbed “wild type” transition state ensemble, and must be excluded from the consensus  $\Phi_M$  analysis of hPin1 WW transition state structure.

**Figure 4: Analysis of the folding transition state of the hPin1 WW domain. (A)**  $\Phi_M$  values of the 34 single and double mutants (dark grey) and the 5 amide-to-ester backbone hydrogen bonds mutants (light grey) that qualify for  $\Phi_M$  analysis, and that were used for consensus  $\Phi_M$  mapping of the folding transition state. **(B)**  $\Phi_M$  map of the folding transition state, with  $\Phi_M$  values for 25 of the 34 residues (single letter representation) mapped onto the C- $\alpha$  backbone structure of the N-terminally truncated folded protein (residues 6-39). Left panel: residues W11-W34 that define the 3-stranded  $\beta$  sheet. Right panel: Residues L7-P37 that includes hydrophobic cluster 1 and the N- and C-terminal extensions. For clarity,  $\Phi_M$  values were grouped and color-coded ( $0 < \Phi_M < 0.30$ , blue;  $0.3 < \Phi_M < 0.6$ , purple,  $0.6 < \Phi_M < 0.90$ , pink;  $\Phi_M > 0.90$ , red). Residues for which classical hydrophobic deletion mutagenesis yields very high, or negative,  $\Phi_M$  values that are not supported by other mutations or structural context are color coded black. Residues for which no mutant suitable for  $\Phi_M$  analysis is available are color coded white. Backbone hydrogen bonds that were studied by amide-to-ester mutagenesis are indicated by arrows (same color code as for side chains). Data used to render the figure are provided in Tables 1 and 2.

**Figure 5:  $\Phi_M$  vs sequence map and  $\Phi_M$  vs backbone disorder correlation (A)** Plot of  $\Phi_M$  values vs. the hPin1 WW sequence used for transition state analysis. Individual side chain  $\Phi_M$  values

are color coded red, while those calculated from backbone hydrogen bond mutants are color-coded blue. The solid red line represents the error-weighted average trend of the side chain  $\Phi_M$  (see Table 2 for data). **(B)** Tube plot showing the distribution of thermal B factors from the X-ray crystal structure [47] along the backbone of hPin1 WW domain. **(C)** Plot of thermal B factors vs. the hPin1 WW sequence, showing a pronounced maximum in loop 1, and a smaller maximum in loop 2. **(D)** Correlation between  $\Phi_M$  values and thermal B factors for residues M15-R21 with increased local backbone disorder at 55 °C. Side chain (sc) loop 1 mutants are color coded red and backbone hydrogen bond mutants (hb) are color coded blue. The solid lines represent best fits of the experimental data.

**Figure 6: Variation of transition state structure with temperature:** **(A)** Plot of  $\Phi_M$  (60 °C) vs  $\Phi_M$  (50 °C). On average,  $\Phi_M$  values increase by 0.07 units when raising the temperature from 50 °C to 60 °C, suggesting that the transition state overall gains native structure upon heating. **(B)** Plot of  $\Phi_T$  (60 °C) vs  $\Phi_T$  (50 °C). On average,  $\Phi_T$  values increase by 0.15 units when raising the temperature from 50 °C to 60 °C, suggesting that the transition state becomes more native-like at elevated temperature, consistent with Hammond's postulate. **(C)** Plot of the  $\Phi_M$  (60 °C)/  $\Phi_M$  (50 °C)-ratio vs the residue number of the hPin1 WW sequence. Data from individual side chain mutants are color coded red. Data from individual backbone hydrogen bond mutants are color coded blue. The solid red line represents the error-weighted average side chain trend. For clarity, the side chain data of E12 (large errors, see Table 2) are not shown.

**Figure 7: Average number of native contacts in the folding transition state.** **(A)** Slope of the ground state free energy ( $\partial\Delta G_{\text{ground}}(T)/\partial T$ ) of the 39 consensus mutants used for  $\Phi_M$  analysis (filled red circles, solid black line) or the entire set of single and double mutants (excluding the 6 loop 1 insertion and deletion variants) (filled grey circles, dashed black line) at the midpoint of unfolding ( $T = T_m$ , with  $\Delta G_{\text{ground}}(T_m) = 0$ ). **(B)** Corresponding plot as in (A) showing the slope of the free energy of activation ( $\partial\Delta G_{\text{activated}}(T)/\partial T$ ) at the midpoint of unfolding ( $T = T_m$ ). The ratio of the two slopes (activated/ground) of  $\sim 0.70$  for the 39 consensus mutants (0.63 for the entire

mutant set) suggests that about 70 % of the native contacts are developed in the folding transition state, a value that agrees well with the average calculated from the  $\Phi_M$  data (Table 2), but that is higher than the average  $\Phi_T$  value (0.50). The loop 1 insertion and deletion variants that change local changes in backbone topology (filled yellow circles) were excluded from the fit, but their values agree well with the extrapolated fits of the mutants with the 6-residue wild type hPin1 WW loop 1.

**Figure 8:  $\Phi_M$  analysis of hPin1 WW variants with loop 1 deletions or insertions mutations. (A)**

Loop 1 sequences of the hPin1 WW loop 1 deletions or insertions variants. Wild type residues are numbered and color coded grey. Mutated or deleted residues in the loop deletion variants are color coded red (type-I G-bulge turn) and blue (type-I' turn), while the inserted Gly residues in the loop 1 insertion mutants are highlighted in orange. **(B)** Superposition of the high resolution X-ray structures of type-I G-bulge variant FiP ( 1.90 Å resolution, color coded red, left) and the type-I' variant 3 (1.50 Å resolution, color coded blue, right) with wild type hPin1 WW structure (1.35 Å resolution, color coded grey). **(C)** Brønsted plot for folding of the loop 1 variants of hPin1 WW at 60 °C, rendered from the data provided in SI Table 2. Filled red circles: 5-residue type-I G-bulge turn mutants (var1, var2). Filled blue circles: 4-residue type-I' turn variants (var3, var4). Filled green circles: Cross-validated loop 1 side chain and backbone hydrogen bond mutants (6-residue wild type loop 1 context). Filled orange circles: Gly insertion variants (var5, var6). Filled black circles: Outlier/perturbing mutants. Open light grey circles: Non-loop 1 consensus mutants. The solid black line is the line predicted for  $\Phi_M = 1$ . **(D)** Bar plot of  $\Phi_M$ -values for selected mutants shown in (C).  $\Phi_M$  values calculated for the redesigned loop 1 variants using wild type hPin1 WW as reference are color coded red (5-residue type-I G-bulge variants) and blue (4-residue type-I' variants).  $\Phi_M$  values calculated for variants 2 and 4 in the type-I G-bulge (var1, FiP) and type-I' context (var3) are shown in light red and light blue, respectively.

**Figure 9: Hypothetical “hybrid”  $\Phi_M$  map for the fast-folding FiP variant of hPin1 WW.**

Hypothetical side chain  $\Phi_M$  map (red circles and solid red line) for the fast folding FiP variant of

hPin1 WW, rendered with side chain  $\Phi_M$  values of non-loop 1 mutants measured with wild type hPin1 WW as reference (see Fig. 3, SI Table 2 for details) and the side chain  $\Phi_M$  value for loop 1 FiP WW variant 2 (loop 1 sequence: SSSGR) measured with FiP as “pseudo wild type” reference (loop 1 sequence: SADGR). As two residues were replaced simultaneously in FiP variant 2 (A18S, D19S, see Fig. 8A), the  $\Phi_M$  value calculated for variant 2 ( $\Phi_M = 0.94 \pm 0.05$ ) was assigned to either mutated residue (labeled by asterisks) in FiP. For residues that are probed by multiple side chain mutations, the error-weighted average  $\Phi_M$  value is shown (see SI Table 2 for details). Experimentally measured backbone hydrogen bond  $\Phi_M$  values (filled yellow squares) are those measured for wild type hPin1 WW and are assigned to the two residues that engage in the perturbed hydrogen bond (see SI Table 2 for details). The simulated side chain and backbone hydrogen bond  $\Phi_M$  values and associated errors are shown in green and blue, respectively and were rendered from Fig. 2E in [14]. Residue numbers correspond to the 33-residue FiP sequence and thus account for the shorter loop 1 substructure (deletion of Arg17 of wild type hPin1 WW).



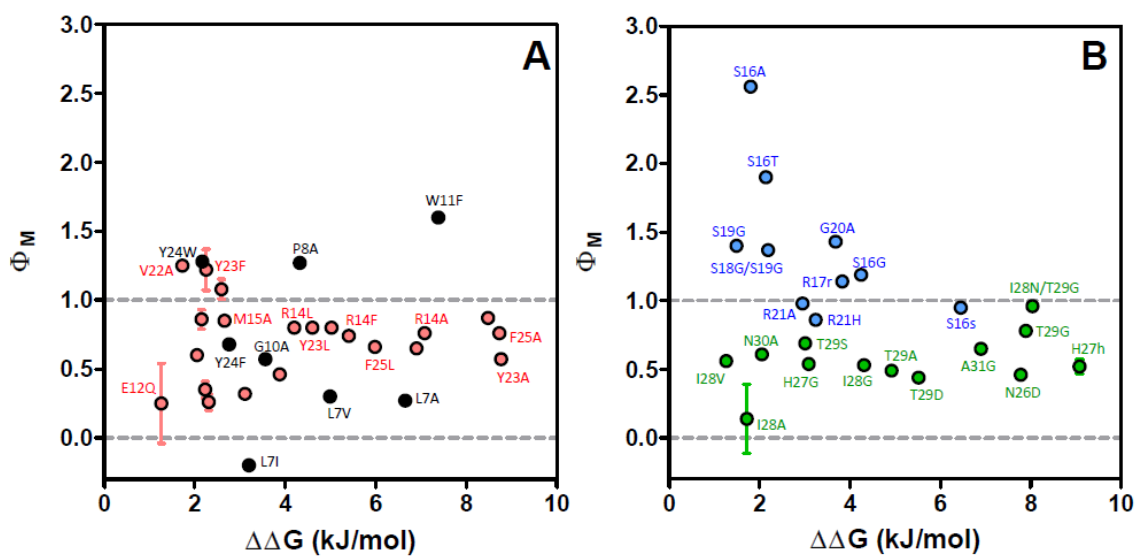


Fig. 2

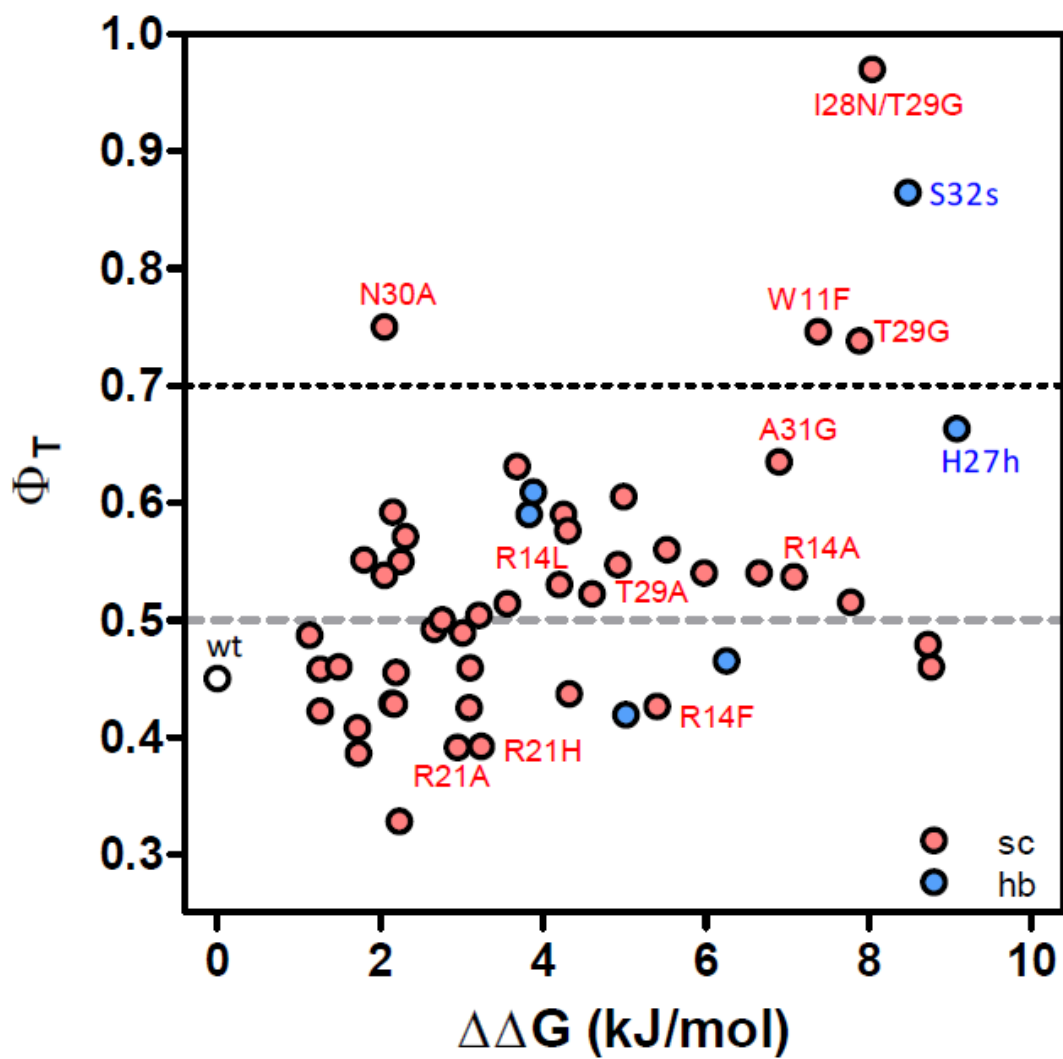


Fig. 3

A

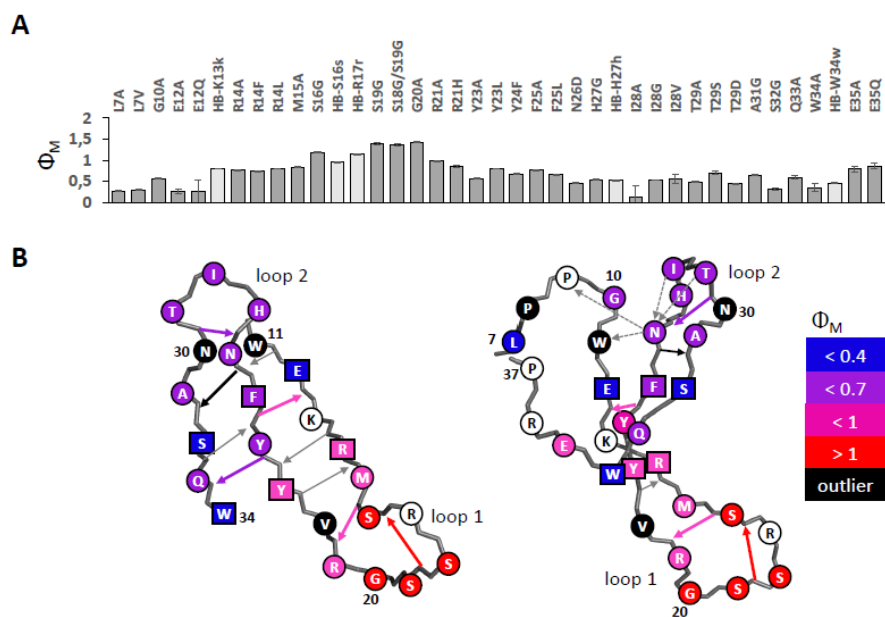


Fig. 4

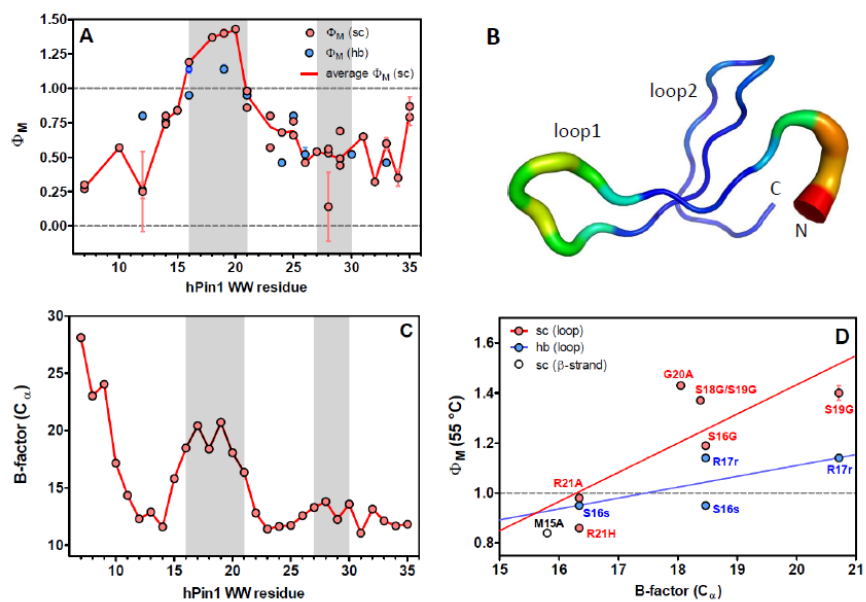


Fig. 5

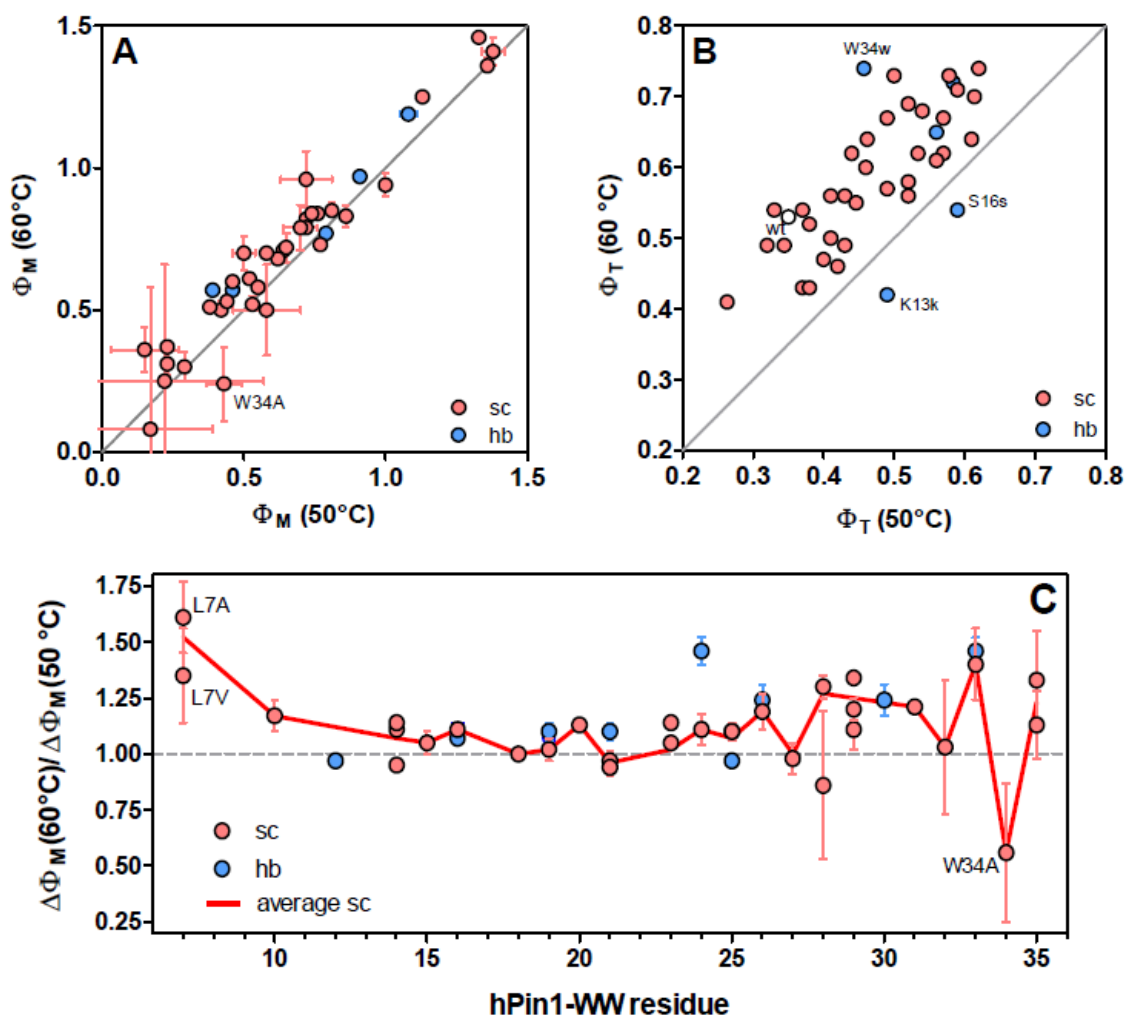


Fig. 6

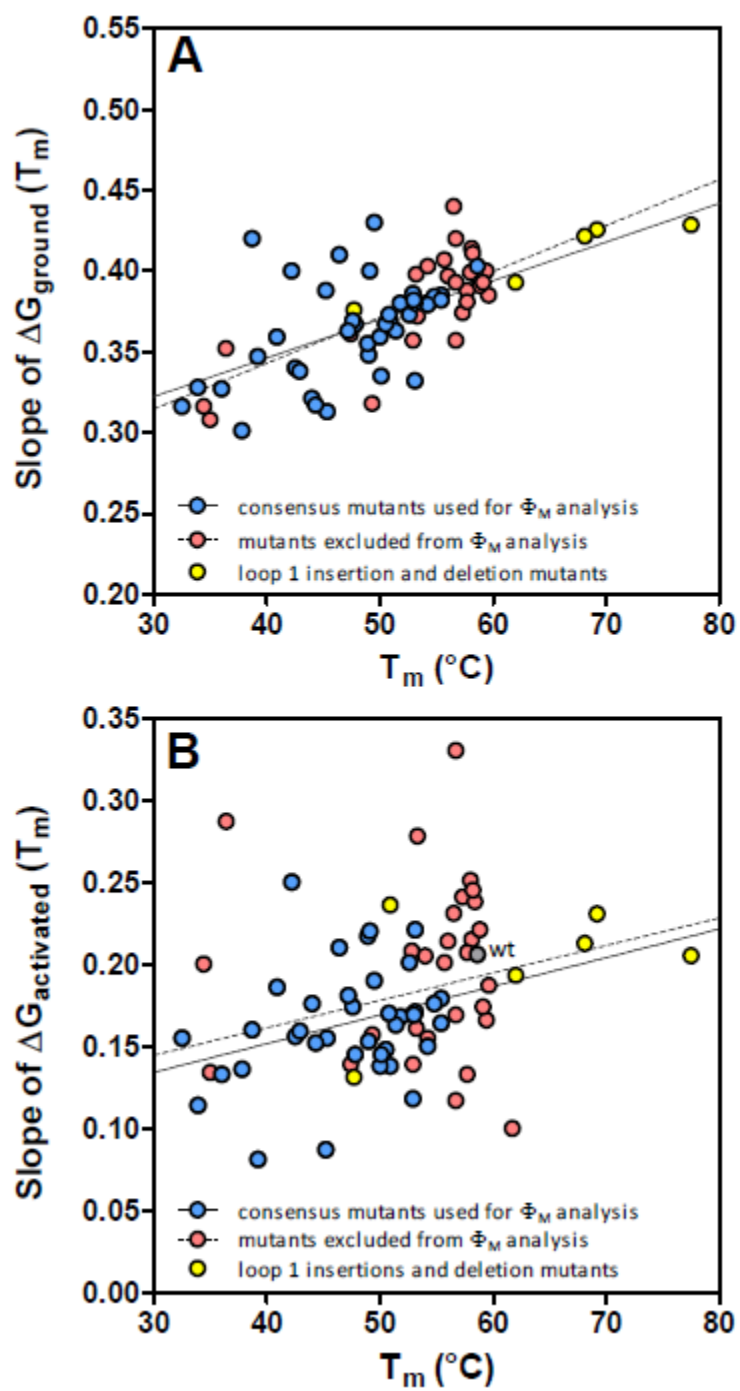


Fig. 7

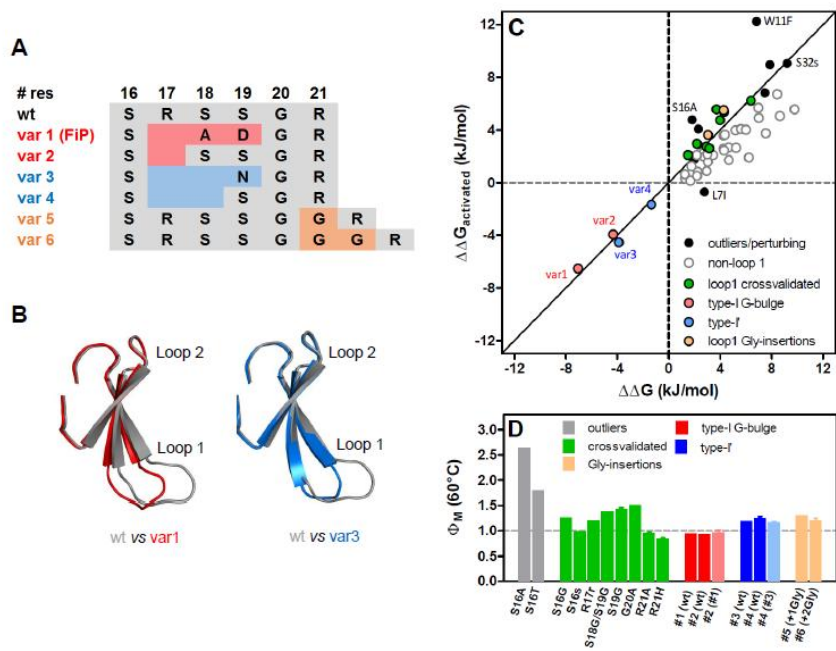


Fig. 8

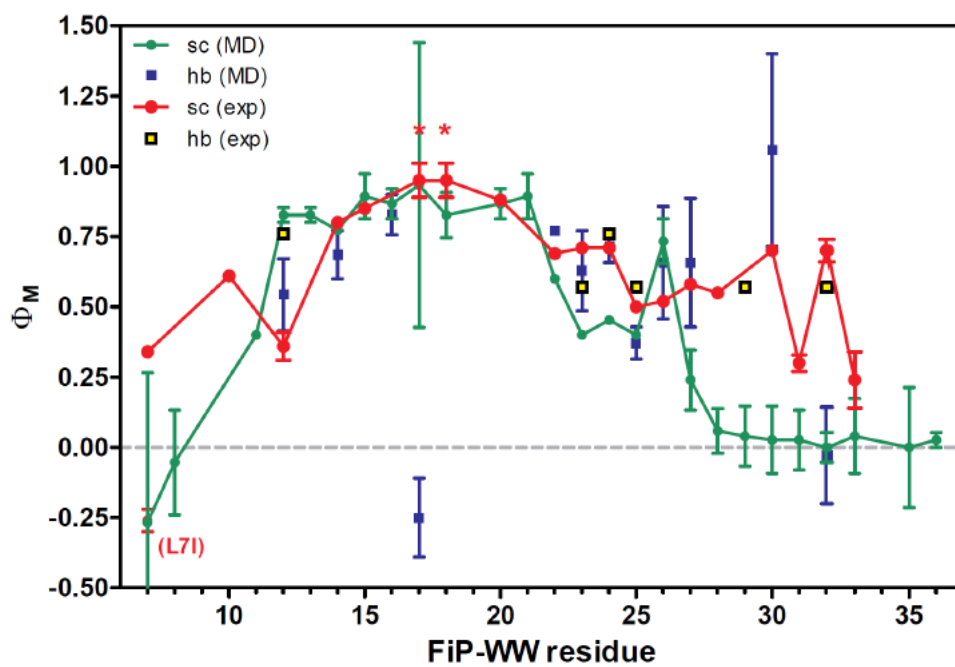


Fig. 9



## Tables (main text)

**Table 1:** Thermodynamic and kinetic data for wild type hPin1 WW and mutants thereof

Variant	$T_m$ (°C)	$\Delta G_f^{(1)}$	$\Delta G_f^{(2)}$	$\Delta G^{†(0)}$	$\Delta G^{†(1)}$	$\Delta G^{†(2)}$	$\Phi_M$ (50 °C) <sup>1</sup>	$\Phi_M$ (55 °C) <sup>1</sup>	$\Phi_M$ (60 °C) <sup>1</sup>	Ref.
<i>1. Wildtype and single-site mutants</i>										
wt hPin1	58.6	0.403	0.00272	14.92	0.206	0.00472	-	-	-	[10]
K6A	59.4	0.400	0.00153	11.16	0.166	0.00173	-	-	-	[10]
K6M	58.1	0.414	0.00180	11.76	0.215	0.00162	-	-	-	N <sup>3</sup>
L7A	37.8	0.301	0.00022	13.16	0.136	0.00192	0.23 (0.02)	0.27 (0.02)	0.31 (0.03)	[6, 10]
L7I	49.3	0.318	0.00050	12.66	0.157	0.00141	-0.21 (0.04)	-0.20 (0.04)	-0.26 (0.04)	[10]
L7V	44.0	0.321	0.00041	13.56	0.176	0.00218	0.23 (0.02)	0.30 (0.02)	0.37 (0.02)	[10]
P8A	47.4	0.361	0.00293	18.56	0.139	0.00237	1.29 (0.01)	1.27 (0.01)	1.23 (0.01)	[10]
P9A	56.0	0.397	0.00229	19.10	0.214	0.00272	-	-	-	[10]
G10A	49.0	0.348	0.00151	15.23	0.153	0.00341	0.52 (0.02)	0.57 (0.02)	0.61 (0.02)	[10]
W11F	3.05	0.308	-0.00050	21.62	0.134	0.00399	1.42 (0.01)	1.58 (0.01)	1.79(0.01)	[10]
E12A	52.6	0.373	0.00104	14.33	0.201	0.00396	0.15 (0.12)	0.26 (0.06)	0.36 (0.05)	[10]
E12Q	55.4	0.385	0.00308	14.62	0.179	0.00421	0.22 (0.35)	0.25 (0.30)	0.25 (0.29)	[6, 10]
K13A	59.6	0.385	0.00285	16.11	0.187	0.00139	-	-	-	[10]
K13V	62.8	0.401	0.00322	15.85	0.215	0.00213	-	-	-	N
K13Y	51.7	0.349	0.00237	16.63	0.125	0.00120	1.09 (0.07)	1.09 (0.07)	1.01 (0.08)	N
R14A	39.2	0.347	0.00074	17.21	0.081	0.00464	0.72 (0.01)	0.76 (0.01)	0.82 (0.01)	[10]
R14F	45.2	0.388	0.00195	16.87	0.087	0.00517	0.76 (0.01)	0.74 (0.01)	0.73 (0.01)	[6]
R14L	47.8	0.367	0.00234	16.31	0.145	0.00482	0.77 (0.01)	0.80 (0.01)	0.84 (0.01)	N
M15A	51.8	0.380	0.00289	15.88	0.168	0.00434	0.81 (0.02)	0.84 (0.02)	0.85 (0.02)	[6, 10]
S16A	54.0	0.380	0.00313	18.63	0.205	0.00372	2.44 (0.03)	2.56 (0.02)	2.62 (0.02)	[10]
S16G	47.6	0.369	0.00194	17.75	0.174	0.00452	1.13 (0.01)	1.19 (0.01)	1.25 (0.01)	[10]
S16T	53.2	0.398	0.00325	18.01	0.161	0.00401	1.99 (0.02)	1.90 (0.02)	1.78 (0.01)	[6]
R17A	58.8	0.391	0.00232	19.23	0.221	0.00276	-	-	-	[10]
R17G	57.3	0.374	0.00277	18.76	0.241	0.00301	-	-	-	[10]
S18A	58.4	0.398	0.00185	22.34	0.238	0.00614	-	-	-	[10]
S18G	56.5	0.440	0.00227	16.49	0.231	0.00670	-	-	-	[10]
S19G	54.8	0.384	0.00248	16.29	0.176	0.00432	1.38 (0.04)	1.40 (0.01)	1.41 (0.04)	[6, 10]
G20A	48.9	0.355	0.00270	18.11	0.217	0.00216	1.33 (0.01)	1.43 (0.01)	1.50 (0.01)	[10]
R21A	50.9	0.369	0.00144	16.54	0.138	0.00181	1.00 (0.02)	0.98 (0.02)	0.94 (0.02)	[10]
R21H	50.0	0.359	0.00130	16.31	0.138	0.00127	0.86 (0.02)	0.86 (0.02)	0.83 (0.02)	N
R21L <sup>4</sup>	55.9	0.521	-0.00010	15.63	0.217	0.00111	-	-	-	N
V22A	54.2	0.403	0.00116	16.29	0.155	0.00146	1.36 (0.05)	1.25 (0.04)	1.12 (0.04)	[6, 10]
Y23A	33.9	0.328	0.00098	15.99	0.114	0.00193	0.55 (0.01)	0.57 (0.01)	0.58 (0.01)	[10]
Y23F	52.8	0.376	0.00254	16.54	0.208	0.00141	1.11 (0.02)	1.23 (0.02)	1.27 (0.02)	[10]
Y23L	45.3	0.313	0.00153	16.24	0.155	0.00159	0.74 (0.01)	0.80 (0.01)	0.84 (0.01)	[6, 10]
Y24F	51.4	0.363	0.00279	15.49	0.163	0.00392	0.64 (0.02)	0.68 (0.02)	0.71 (0.02)	[10]
Y24W	52.9	0.357	0.00230	16.72	0.139	0.00436	1.27 (0.02)	1.28 (0.02)	1.30 (0.02)	[10]
F25A	32.5	0.316	0.00042	16.92	0.155	0.00098	0.72 (0.01)	0.76 (0.02)	0.79 (0.02)	[10]
F25L	42.5	0.340	0.00202	15.85	0.156	0.00239	0.62 (0.01)	0.66 (0.01)	0.68 (0.01)	[6, 10]
N26D	36.0	0.327	0.00044	14.56	0.133	0.00211	0.42 (0.01)	0.46 (0.02)	0.50 (0.03)	[6, 10]
H27A	57.7	0.388	0.00262	14.76	0.207	0.00245	-	-	-	[10]
H27G	50.5	0.367	0.00130	15.20	0.148	0.00197	0.53 (0.02)	0.54 (0.02)	0.52 (0.02)	[10]
I28A	54.2	0.379	0.00165	14.35	0.150	0.00404	0.17 (0.22)	0.14 (0.25)	0.08 (0.44)	[6, 10]

I28G	47.2	0.363	0.00105	14.93	0.181	0.00326	0.46 (0.01)	0.53 (0.01)	0.60 (0.01)	[10]
I28V	55.4	0.382	0.00328	15.01	0.164	0.00413	0.58 (0.12)	0.56 (0.10)	0.50 (0.12)	[10]
T29A	44.3	0.317	0.00100	14.80	0.152	0.00205	0.44 (0.01)	0.49 (0.01)	0.53 (0.01)	[10]
T29D	42.9	0.338	0.00009	14.38	0.159	0.00262	0.38 (0.01)	0.44 (0.01)	0.51 (0.01)	[6]
T29G	34.4	0.316	0.00001	15.32	0.200	0.00243	0.68 (0.01)	0.79 (0.01)	0.91 (0.02)	[10]
T29S	50.8	0.373	0.00159	15.57	0.170	0.00278	0.65 (0.03)	0.70 (0.03)	0.72 (0.04)	[10]
N30A	53.3	0.372	0.00208	15.02	0.278	0.00302	0.31 (0.07)	0.61 (0.03)	0.89 (0.03)	[10]
A31G	40.9	0.359	0.00197	15.45	0.186	0.00311	0.58 (0.01)	0.65 (0.01)	0.70 (0.01)	[6, 10]
A31S	57.7	0.381	0.00283	15.76	0.133	0.00373	-	-	-	[10]
S32G	50.1	0.335	0.00200	14.46	0.145	0.00198	0.29 (0.03)	0.32 (0.03)	0.30 (0.04)	[10]
S32T	61.7	0.398	0.00356	14.70	0.100	0.00240	-	-	-	[6]
Q33A	53.1	0.332	0.00103	15.13	0.171	0.00326	0.50 (0.04)	0.60 (0.04)	0.70 (0.04)	N
W34A	52.9	0.386	0.00067	14.75	0.118	0.00295	0.43 (0.06)	0.35 (0.06)	0.24 (0.10)	[6, 10]
W34F	58.0	0.399	0.00326	15.81	0.251	0.00212	-	-	-	[10]
E35Q	53.1	0.380	0.00280	15.67	0.221	0.00265	0.72 (0.09)	0.87 (0.06)	0.96 (0.06)	[10]
E35A	50.3	0.369	0.00283	16.13	0.154	0.00203	0.82 (0.07)	0.83 (0.07)	0.79 (0.06)	[10]
R36A	56.7	0.357	0.00225	16.44	0.117	0.00231	-	-	-	[10]
S38A	59.1	0.393	0.00204	17.13	0.174	0.00327	-	-	-	[10]
S38G	58.2	0.411	0.00382	18.43	0.245	0.00295	-	-	-	[10]
S38T	58.2	0.390	0.00327	18.22	0.232	0.00337	-	-	-	N

#### 2. Double-site mutants

S18G/S19G	53.0	0.382	0.00163	16.88	0.169	0.00246	1.36 (0.02)	1.37 (0.02)	1.36 (0.02)	N
S19G/G20S	56.7	0.393	0.00288	16.88	0.169	0.00246	-	-	-	N
I28N/T29G	36.4	0.352	0.00024	15.25	0.287	0.00387	0.79 (0.01)	0.96 (0.01)	1.14 (0.01)	N

#### 3. Loop1 insertion and deletion mutants<sup>2</sup>

var1 (FIP)	77.5	0.428	0.00327	10.65	0.2052	0.00532	-	-	0.92 (0.01)	[7]
var2	69.2	0.425	0.00191	13.01	0.2305	0.00457	-	0.84 (0.01)	0.91 (0.01)	[7]
var3	68.1	0.422	0.00220	12.07	0.2126	0.00498	-	-	1.18 (0.01)	[7]
var4	62.0	0.393	0.00228	13.92	0.1931	0.00216	-	1.28 (0.07)	1.24 (0.04)	[7]
var5 (+1G)	47.7	0.396	0.00139	18.73	0.1310	0.00256	1.34 (0.01)	1.32 (0.01)	1.32 (0.01)	N
var6 (+2G)	50.9	0.366	0.00347	16.47	0.2360	0.00281	0.94 (0.01)	1.09 (0.01)	1.09 (0.01)	N

#### 4. Backbone hydrogen bond amide-to-ester mutants

K13k	46.4	0.410	0.0010	16.52	0.21	0.00100	0.79 (0.01)	0.80 (0.01)	0.77 (0.01)	[16]
S16s	42.2	0.400	-0.0005	17.37	0.25	0.00120	0.91 (0.01)	0.95 (0.01)	0.97 (0.01)	[16]
R17r	49.1	0.400	0.0016	17.20	0.22	0.00300	1.08 (0.03)	1.14 (0.03)	1.19 (0.03)	[16]
V22v	56.7	0.420	0.0034	16.64	0.33	0.00340	-	-	-	[16]
H27h	38.7	0.420	0.0031	14.83	0.16	0.00560	0.46 (0.01)	0.52 (0.01)	0.57 (0.01)	[16]
S32s	41.5	0.510	0.0010	14.70	0.50	0.00090	0.72 (0.01)	0.87 (0.01)	0.98 (0.01)	[16]
W34w	49.5	0.430	0.0032	14.74	0.19	0.00840	0.39 (0.03)	0.46 (0.02)	0.57 (0.01)	[16]

<sup>1</sup> Mutants that differ < 1 kJ/mole in stability from wild type hPin1 WW resulted in large errors in  $\Phi_M$ , so no  $\Phi_M$ -values are listed.  $\Phi_M$ -value were also not calculated at 50 and/or 55 °C for the more stable loop 1 deletion mutants with thermodynamically optimized loop 1 substructures, to avoid errors in  $\Phi_M$  due to extrapolation of the data. Rounded errors in  $\Phi_M$  of all other mutants are given in brackets.

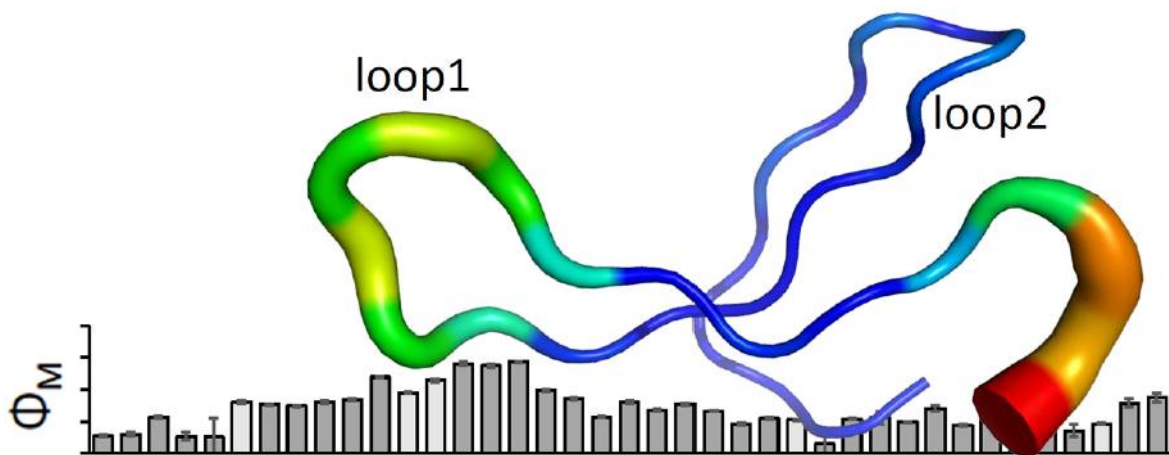
<sup>2</sup> Var1: Type-I G-bulge turn, sequence: SADGR. Var2: Type-I G-bulge turn, sequence: SSSGR. Var3: Type-I' turn, sequence: SNGR. Var4: Type-I' turn, sequence: SSSGR. Var5: Single Gly insertion, sequence: SRSSGGR. Var6: Double Gly insertion, sequence: SRSSGGGR. <sup>3</sup> N= new mutant.

<sup>4</sup> Mutant R21L forms a dimer at protein concentrations employed for T-jump relaxation (10-30  $\mu$ M) and was thus excluded from  $\Phi_M$  analysis.

**Table 2:** Summary of  $\Phi_M$  values of consensus mutants used for transition state mapping at 55 °C

Residue	Mutation	Type <sup>1</sup>	$\Delta\Delta G$ (kJ/mol)	$\Phi_M$ (55 °C)	Average $\Phi_M$ (sc)	Average $\Phi_M$ (hb)
L7	L7A	sc	6.65	0.27 (0.02)	0.28	-
	L7V	sc	5.00	0.30 (0.02)		
G10	G10A	sc	3.56	0.57 (0.02)	0.57	-
E12	E12A	sc	2.31	0.26 (0.06)	0.26	0.80
	E12Q	sc	1.26	0.25 (0.29)		
	K13k	hb	5.01	0.80 (0.01)		
R14	R14A	sc	7.08	0.76 (0.01)	0.77	-
	R14F	sc	5.41	0.74 (0.01)		
	R14L	sc	4.18	0.80 (0.01)		
M15	M15A	sc	2.66	0.84 (0.02)	0.84	-
S16	S16G	sc	4.25	1.19 (0.01)	1.19	1.01
	S16s	hb	6.45	0.95 (0.01)		
	R17r	hb	3.38	1.14 (0.02)		
S18 <sup>3</sup>	S18G/S19G	sc	2.19	1.37 (0.02)	1.37	-
S19	S19G	sc	1.49	1.40 (0.03)	1.40	1.19
G20	G20A	sc	3.68	1.43 (0.01)	1.42	-
R21	R21A	sc	2.95	0.98 (0.02)	0.92	0.95
	R21H	sc	3.24	0.86 (0.02)		
Y23	Y23A	sc	8.77	0.57 (0.01)	0.72	-
	Y23L	sc	4.60	0.80 (0.01)		
Y24	Y24F	sc	2.76	0.68 (0.02)	0.68	0.46
F25	F25A	sc	8.73	0.76 (0.02)	0.69	0.80
	F25L	sc	5.98	0.66 (0.01)		
N26	N26D	sc	7.79	0.46 (0.02)	0.46	0.52
	H27h	hb	9.08	0.52 (0.01)		
H27	H27G	sc	3.09	0.54 (0.02)	0.54	-
I28	I28A	sc	1.72	0.14 (0.25)	0.52	-
	I28V	sc	1.26	0.56 (0.10)		
	I28G	sc	4.31	0.53 (0.01)		
T29	T29A	sc	4.92	0.49 (0.01)	0.49	-
	T29S	sc	3.01	0.70 (0.04)		
	T29D	sc	5.52	0.44 (0.01)		
N30	H27h	hb	9.08	0.52 (0.01)	-	0.52
A31	A31G	sc	6.87	0.65 (0.01)	0.65	-
S32	S32G	sc	3.10	0.32 (0.03)	0.32	-
Q33	Q33A	sc	2.05	0.60 (0.04)	0.60	0.46
	W34w	hb	3.87	0.46 (0.01)		
W34	W34A	sc	2.23	0.35 (0.10)	0.35	-
E35	E35A	sc	3.27	0.83 (0.06)	0.85	-
	E35Q	sc	2.14	0.87 (0.07)		

<sup>1</sup>Type of mutation: side chain (sc), backbone hydrogen bond (hb). <sup>2</sup> Error weighted average  $\Phi_M$ -value for residues probed by multiple mutations. <sup>3</sup>  $\Phi_M$ -value of the S18G/S19G was assigned to S18.



Graphical abstract

ACCEPTED MANUSCRIPT

### Highlights

- Folding kinetics of a comprehensive set of hPin1 WW mutants, spanning the whole sequence and multiple substitutions at many sites, has been studied.
- A very conservative phi value analysis, identifying and excluding disruptive mutations, has revealed the interplay between loops 1 and 2 in the transition state in unprecedented detail.
- Unusually large “non-classical” phi values are now explained by local native state disorder.
- This comprehensive experimental data set will be valuable for comparison with molecular dynamics simulation, and we begin by creating a hybrid Phi-value map for FiP WW domain for comparison with recent all-atom simulations.

ACCEPTED MANUSCRIPT